Available online at www.CivileJournal.org

Civil Engineering Journal

Vol. 5, No. 2, February, 2019

# Investigating the Behavior of Buildings under the Effect of the New Design Ground Motion of Iraq

Mustafa Shakir Farman [a*], AbdulMuttalib Isa Said [b]

[a] *Faculty Member, Building and Construction Department, Technical Institute of Samawa, Al-Furat Al-Awsat University, Kufa, Iraq.*

[b] *Professor, Faculty Member, Civil Engineering Department, University of Baghdad, Baghdad, Iraq.*

Received 20 September 2018; Accepted 27 January 2019

**Abstract**

Recently, Iraq has experienced an increase in seismic activity, especially, near the east boundary with Iran which enhanced the need to study its effect on the behavior of buildings. In this study, a comprehensive methodology was applied to investigate the behavior of a moment frame system with respect to its height after subjected to the design ground motion at Baghdad according to the recently developed seismic hazard maps and, after developing and designing the required configurations of archetype models, specifying life safety as an aimed performance level, modeling nonlinearity and applying the nonlinear static analysis (NSP) according to ASCE/SEI41-13, FEMA356 and FEMA P-695. This methodology is started by sizing members cross-sectional dimensions and applying reinforcement detailing requirements according to ACI318-14. Results show that, for a given building height and number of bays, inelastic drifts increase with decreasing the bay width because the overall building stiffness is decreased and it will be more slender, and consequently, the P- delta effects increased. Also, as the building height increased, both, target and minimum shear capacities decrease and the target displacement increases under the effect of the same earthquake ground motion. Consequently, a necessary limitation on the height of these buildings were deduced to ensure their ability to withstand the future ground shaking and, in the same time, maintaining the life safety performance level of damage. Where, it is found that the maximum allowed heights of framed buildings in Baghdad are 17, 25 and 32 stories for 6, 7.5 and 9 m bay widths, respectively.

*Keywords:* NSP; Baghdad; Moment Frame System; Inelastic Drifts; Shear Capacity; Height.

## 1. Introduction

Recently, Iraq has experienced an unprecedented seismic activity, specifically, near the east boundary with Iran which pushed towards re-evaluating the seismic hazard at this region. The most recent studies were made by AbdulMuttalib et al. (2018) and Mustafa et al. (2018), where the PGA and spectral accelerations at 0.2 second and 1.0 second were presented in the form of contour maps. Also, they presented the future forecasting design response spectrum of the main cities in Iraq [1, 2]. Their findings showed that the future forecasting earthquakes will be increased towards the east-northeast and north, therefore, there is a big need for investigating the performance of the seismic-force resisting system under the effect of the future forecasting earthquakes.

In order to apply the analysis and study the performance of any seismic-force resisting system under the effect of the future forecasting earthquake, the structure, foundation and loading of building need to be modeled. Moment frames are generally selected as the seismic force- resisting system when architectural space planning flexibility is desired [3]. Among the types of moment frames, the special Moment frame is the only one can be used for all Seismic Design Categories especially Categories D, E and F of ASCE/ SEI 7- 05 or Iraqi seismic code, therefore, it is preferred to be

* Corresponding author: alishf2013@yahoo.com

http://dx.doi.org/10.28991/cej-2019-03091261

➢ This is an open access article under the CC-BY license (https://creativecommons.org/licenses/by/4.0/).

© Authors retain all copyrights.

adopted in selecting frame models. In this study, the future forecasting earthquake will be represented by the design response spectrum of Baghdad city from the study of Mustafa Sh. F. and AbdulMuttalib I. S. (2018).

In the Iranian code of practice (2007) the maximum permissible building height for Special reinforced concrete moment- resisting frames (SMRFs) is 150 m. Also, the performance factor R is Equals to 10 [6].

In Turkish earthquake code TEC (2007) the reinforced concrete moment frames of nominal ductility in the two directions or in one and the other is of high ductility, are permitted to be used with a height not exceeding 25 m. Also, the Seismic Performance Factor, (R), for frames of nominal ductility is differ than that in frames of high ductility level, which means that R for frames with long periods is differ than that in frames of lower periods, or implicitly R is dependent on building height [7].

In FEMA_P695 (2009) the methodology used to develop the Seismic Performance Factors (R , Ωo, Cd) of ASCE/ SEI 7- 05 for each seismic-force resisting system is presented. In this methodology, a number of archetype configurations are developed which representing the main differences or variations in the framing bay sizes, period or height, the ground motion intensity and other factors that may affect the seismic behavior of the moment frame system. These archetype models are firstly analyzed linearly based on a trial values of (R, Ωo, Cd) same as that in Table (12.2.1) of ASCE/SEI 7- 05 and then designed. After that, the components nonlinearity were modeled and then these archetype nonlinear models were analyzed nonlinearly [8]. Finally, it was found that frames models based on trial constant values from ASCE/ SEI 7- 05 are performed poorly as the height increased. This means, the acceptability of the trial values from ASCE/ SEI 7- 05 was weaker as increasing the height and it was suggested to limit the number of stories to a 12 stories. But they may be accept Table between 12 and 20 stories because the variation of number of stories that represented in the models was only 4, 8, 12 and 20 stories [8].

Haselton and Deierlein (2007) explained that this poor performance is due to the damage localized more for taller moment frames since damage localization is driven mainly by higher P-delta effects as the building height increases. So as to assure better performance in taller reinforced concrete frame buildings strength requirements can be increased for taller buildings, by using a period-dependent R factor [9].

In Indian standard ICS (2016) of tall buildings that are of heights between 45 and 250 m that usually used as office and residential buildings, the moment frame system is permitted to be used only in low and moderate seismic zones with maximum heights not exceeding 80 and 60 m, respectively. Also, the maximum slenderness ratio, that is the building height to smaller plan dimension, is not exceeding 5 and 4 for the low and moderate seismic zones, respectively [10,11].

Increasing the strength or decreasing R with height means mainly increasing columns sections to be as a strong vertical shafts which distribute damages over the building height. But this will conflict with the fact that the column section cannot continue to be increased without limit, in addition to the economic aspect. Instead, the height of a moment frame can be limited up to a level at which a concrete wall needs to be used as a strong vertical shaft which distributes damages over the height. But, this height limit will depend on the bay sizes, sizing the members cross-sectional dimensions, reinforcement details and on the design ground motion. Consequently, the objective of this study is investigating the performance of a moment frame system with respect to its height, this is for a given cases of bay sizes and design ground motion, and based on a robust criteria for sizing the members cross-sectional dimensions and for applying reinforcement detailing requirements. This needs specifying the aimed performance level, modeling and analysis procedure, or in other words specifying the overall methodology used to conduct this study based on known standards and specifications. As a whole, this study is divided into two stages, which are;

a) Preparing and analyzing the nonlinear models of archetypal buildings, which including:

1. Preparation of archetype models.
2. Developing of nonlinear models.
3. Applying the design load combinations.
4. Linearly analyzing and designing the nonlinear models.
5. Applying the Nonlinear Static analysis.

b) Parametric study is to be done to study the effect of height of building (or number of stories), building slenderness ratio (or bay size) and the new seismic hazard maps values for framed buildings in the Baghdad city.

## 2. Preparing and Developing Nonlinear Models

### 2.1. Preparation of Archetype Models

The two-dimensional model presented in Figure 1 is firstly used by Haselton and Deierlein (2007) and will be used here as a basis for sorting the minimum number of archetype configurations comprising the important and satisfying range of reinforced concrete moment frame buildings in this study.

Considering typical office occupancies, three basic configurations of reinforced concrete special moment frame, (SMF), archetypes will be adopted which are 6, 7.5 and 9 m bay widths. This is to cover the range of bay sizes of (6 to 9) m of typical office occupancies [10]. Accordingly, the plan dimensions will be 18m by 18, 22.5 m by 22.5 and 27 m by 27 m. Story heights were taken as 15 feet (≈ 4.5 m), for the first story and 13 feet (≈ 4 m), for the upper stories.

Also for each one of the three basic configurations of a bay size, four primary archetype heights or number of stories were considered, which are 5, 10, 15 and 20 stories, each with a basement of 4 m height. That means the four primary archetype heights are 20.5, 40.5, 60.5 and 80.5 m above ground and 4 m below ground, leading to a total of 12 archetype models, Figure 2.

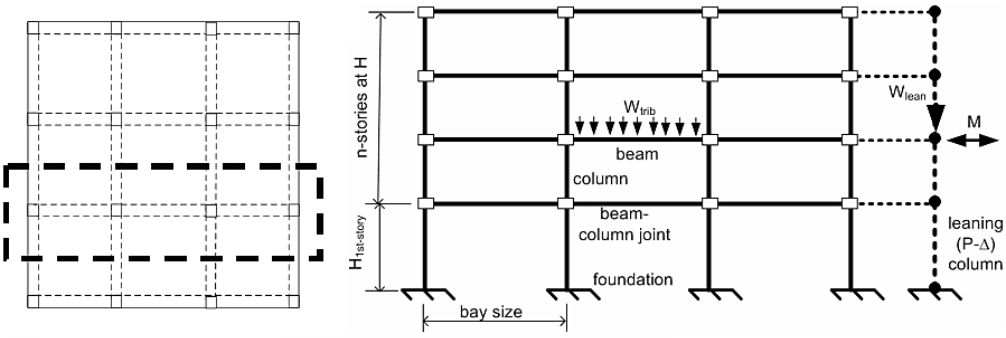


**Figure 1. Archetype model for moment frame buildings [9]**

## 2.2. Design Load Combinations

The combinations of design loads including earthquake effects, according to ASCE/SEI 7-05, ACI 318-14 and Iraqi seismic code that must be used are [4, 12, 5]:

$$U=1.2D+ 1.6L \quad (1)$$

$$U=1.2D+ 0.5L\pm 1.0E \quad (2a)$$

$$U=0.9D\pm1.0E \quad (3a)$$

In case where seismic and gravity load effects are additive:

$$E=\rho Q_E + 0.2S_{DS} D \quad (4)$$

While in the case of counteracting effects of seismic and gravity loads:

$$E=\rho Q_E - 0.2S_{DS} D \quad (5)$$

Equations 2a and 3a will become:

$$U=(1.2+0.2S_{DS} )D + 0.5L \pm \rho Q_E \quad (2b)$$

$$U=(0.9-0.2S_{DS} )D \pm \rho Q_E \quad (3b)$$

Equation 1 represents the design gravity loads only, which will be used to compute the effective stiffness values according to Table 10.5 in ASCE/ SEI 41-13 [13]. According to Section 12.3.4.2b in ASCE/SEI 7-05, the redundancy factor $\rho = 1$. The values of $S_{DS}$ will be taken from Mustafa Sh. F. and AbdulMuttalib I. S. (2018), which is Equals 0.47 for Baghdad city. For Baghdad, Equations (2b, 3b) will become:

$$U=1.294D + 0.5L \pm Q_E \quad (2c)$$

$$U=0.806D \pm Q_E \quad (3c)$$

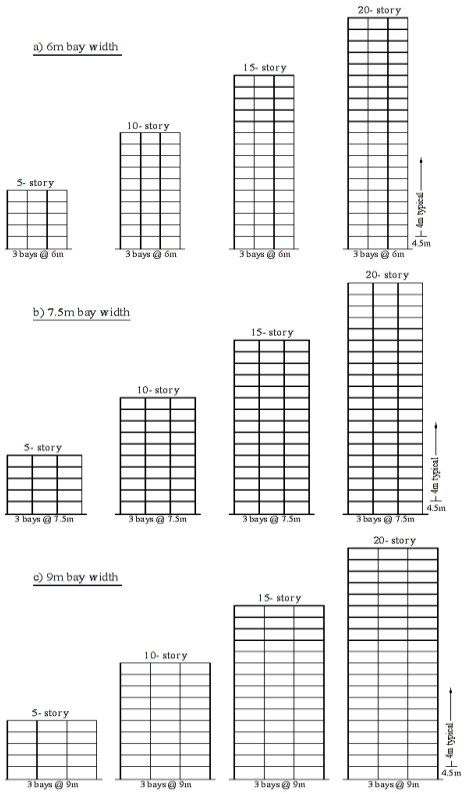


**Figure 2. Archetype configurations for a reinforced concrete moment frame system**

The key design variables identified to have a significant impact on the performance of reinforced concrete moment frame systems, and their applicable ranges, are presented in Table 1 [8].

**Table 1. Summary of key design variables and ranges, and design parameters considered in the design space for reinforced concrete moment frame systems, based on ACI 318-14, ASCE/ SEI 41-13, ASCE/SEI 7-05 and Iraqi seismic code**

| Key design variable | The range considered in the design space of archetype |
|---|---|
| **Configuration** | |
| Special reinforced concrete moment frame (as per ASCE/SEI 7-05, ACI 318-14) | All designs meet code requirements |
| Building height | 5, 10, 15 and 20 stories, in principle |
| Bay width | 6, 7.5 and 9 m |
| First and upper story heights | 4.5 and 4 m |
| **Element design** | |
| Confinement ratio and stirrup spacing | Conforming to ACI 318-14 and ASCE/ SEI 41-13 |
| Concrete compressive strength | 5 ksi (≈34.5 MPa) to 7 ksi (≈48.3 MPa), ACI318-14/ sec.18.7.5.2 and, NIST (2016). |
| Longitudinal bar diameter | Ø18 to Ø32 mm in columns, Ø16 to Ø25 mm in beams |
| **Loading** | |
| Design floor loads | 175 psf (≈ 8.4 kN/ $m^2$ ), [34] |
| Lower and upper bounds on design floor load | 150 to 200 psf (≈ 7.2 to 9.6 kN/ $m^2$ ), [34] |
| Design floor live load | Constant: 50 psf (≈ 2.4 kN/ $m^2$ ) |
| Design roof live load | Constant: 20 psf (≈ 1.0 kN/ $m^2$ ) |
| Design parameter | Design assumption |
| Member stiffness assumed in design: Beams | 0.3EIg, Table 10.5 in ASCE/ SEI 41-13 |
| Member stiffness assumed in design: Columns | Linear interpolation between 0.3EIg and 0.7EIg according to design gravity axial load levels, Table 10.5 in ASCE/ SEI 41-13. |
| Footing rotational stiffness assumed in design | Basement assumed; exterior columns fixed at basement wall, interior columns consider stiffness of first floor beam and basement column. |
| Joint stiffness assumed in design | Extending columns rigidity into joints. |
| SC-WB design principle | Using a minimum ratio of 1.2 |

The design dead load will be taken as an average of 8.4 kN/m$^2$ while the design floor and roof live loads are 2.4 and 1.0 kN/m$^2$, respectively, [8].

ACI 318-14 adopts the (SC-WB) concept by requiring that the ratio of the sum of column moment strengths to the sum of beam moment strengths at their connection joint (ΣMnc / ΣMnb) is not less than 1.2. According to ASCE/ SEI 41-13 and based on Elwood et al. (2007), and for ΣMnc / ΣMnb > 1.2, the joints could be modeled implicitly by extending the column rigidity inside the joint in the mathematical model [13, 14].

## 2.3. Preliminary Proportioning of Members Sections

Proportioning of members sections, especially columns, have an important impact on the response of the archetypes models and thereby final results. Therefore, members sections should be estimated carefully and based on reliable and practical bases. The load combination of Equation 1 represents the design gravity loads only, which will be used preliminarily to proportion columns sections based on the concept that the design axial load Pu is preferred to be:

$$Pu \leq 0.3Ag\ fc' \quad (6)$$

Accordingly, a summary of the preliminary selected columns sections is shown in Table 2. Then, columns sections will be checked, and revised where required to satisfy Equation 6, based on the worst design load combination including seismic load, Equation 2c.

For beams in the first basic archetype configuration of 6m bay width, (6 × 6 m plan panels), the slab thickness has been estimated to be 0.15 m after a preliminary calculations. According to ACI 318-14/ sec.6.3.2.1, the effective flange width of beams is 1.5 m. The depth of beams has preliminarily been selected equals ten percent of the bay size, (0.6 m). Taking into consideration the limits of beams dimensions in ACI 318-14, the web width of beams has been selected to be 0.3 m. Accordingly, The Preliminary sections for beams of the three basic configurations are shown in Figure 3.

**Table 2. Summary of the preliminary selected columns sections**

| Archetypes height steps in terms of number of stories, (*i*) | Column's section depth *h* in meter and values of $f_c'$, *in ksi, for ;* | | | | | | | |
|---|---|---|---|---|---|---|---|---|
| | 5 stories Model | | 10 stories Model | | 15 stories Model | | 20 stories Model | |
| | h | $f_c'$ | h | $f_c'$ | h | $f_c'$ | h | $f_c'$ |
| **Bay width 6 m** | | | | | | | | |
| 16 to 20 | | | | | | | 0.80 | 5 |
| 11 to 15 | | | | | 0.70 | 5 | 0.80 | 5 |
| 6 to 10 | | | 0.60 | 5 | 0.70 | 5 | 0.80 | 6 |
| 1 to 5 | 0.50 | 5 | 0.60 | 6 | 0.70 | 7 | 0.80 | 7 |
| **Bay width 7.5 m** | | | | | | | | |
| 16 to 20 | | | | | | | 1.00 | 5 |
| 11 to 15 | | | | | 0.90 | 5 | 1.00 | 5 |
| 6 to 10 | | | 0.75 | 5 | 0.90 | 5 | 1.00 | 6 |
| 1 to 5 | 0.60 | 5 | 0.75 | 6 | 0.90 | 7 | 1.00 | 7 |
| **Bay width 9 m** | | | | | | | | |
| 16 to 20 | | | | | | | 1.15 | 5 |
| 11 to 15 | | | | | 1.00 | 5 | 1.15 | 5 |
| 6 to 10 | | | 0.85 | 5 | 1.00 | 5 | 1.15 | 6 |
| 1 to 5 | 0.70 | 5 | 0.85 | 7 | 1.00 | 7 | 1.15 | 7 |

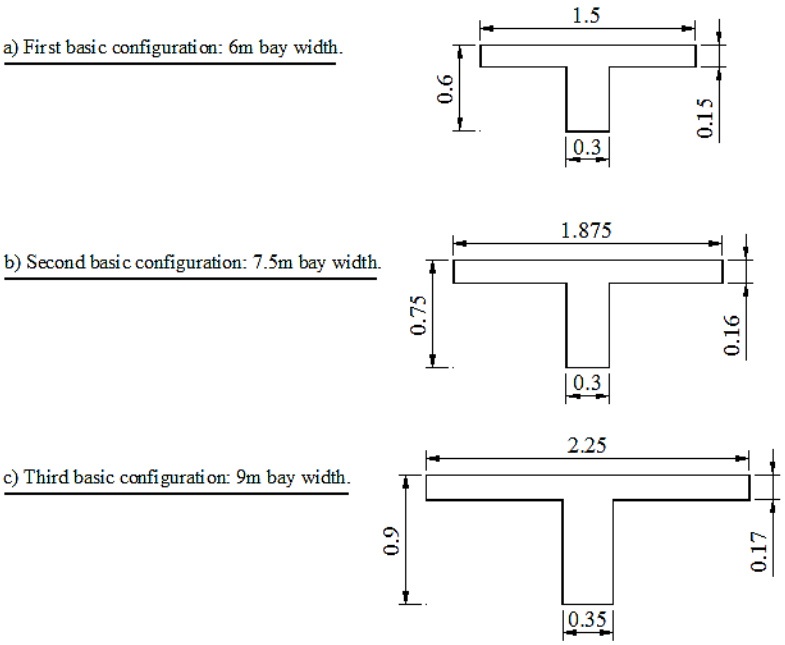


**Figure 3. Preliminary beams sections for the three basic configurations**

The foundations will be modelled so that a basement will be used and the exterior columns will be fixed at basement wall level while the interior columns consider stiffness of basement columns and basement roof beams, which is more realistic. This is according to FEMA_P695.

## 2.4. Linear Analysis and Design of Archetype Models

The Modal Response Spectrum analysis (MRS) method of Section (12.9) in ASCE/SEI 7-05, is preferred to be used in developing archetype designs because the ELF method is not permitted, in some cases, by ASCE/SEI 7-05 and the Iraqi seismic code, for example, in the design of taller buildings in Seismic Design Category D which have a fundamental period, T, greater than 3.5Ts (Table (12.6-1) in ASCE/SEI 7-05), where $Ts=(S_{D1}/S_{DS})$.

The MRS analysis method will be used, with the Seismic Performance Factor R = 8 for SMF from Table (12.2.1) in ASCE/SEI 7-05, to compute the seismic forces needed in the design load combinations of equations (2c and 3c) for Baghdad city.

The MRS analysis and then the design of all archetype models according to the design load combinations of equations (1, 2c and 3c) will be executed by using the program ETABS2016 considering at least 90% mass participation, this is to compute the earthquake load component to be used in the load combinations for seismic design.

From Mustafa Sh. F. and AbdulMuttalib I. S. (2018), $S_{DS}$ and $S_{D1}$ values were 0.47 and 0.25 g for Baghdad. According to ASCE/SEI 7-05 and Iraqi seismic code (2016), the Seismic Design Category SDC will be the more severe one from Tables (11.6.1 and 2) in the ASCE/SEI 7-05, or Tables (2.4.1 and 2) in the Iraqi seismic code (2016). Accordingly, any building in Baghdad will be designed based on SDC D.

## 2.5. Modeling Nonlinearity of Members

According to ASCE/ SEI 41-13, FEMA 356 (2000) and Peer/ ATC-72-1, and after assigning their effective stiffness, columns and beams will be modeled as elastic elements having concentrated plastic hinges at each end, [13, 18, 19]. These plastic hinges are defined by the generalized load-deformation relation shown in Figure 4.

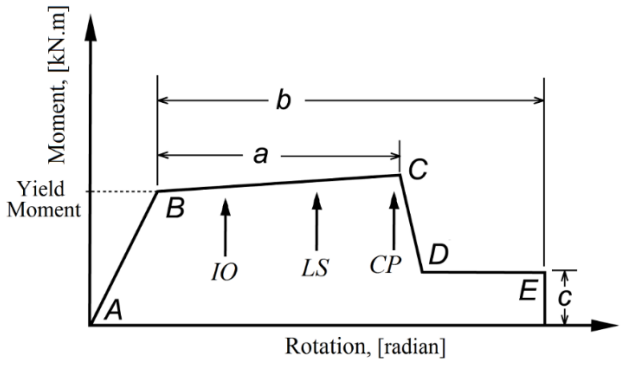


**Figure 4. Generalized component load-deformation relation for nonlinear analysis showing performance levels [13]**

The modeling parameters a, b and c of Figure 4 and the numerical acceptance criteria at different structural performance levels for nonlinear components are provided in Tables (10.7) and (10.8) of ASCE/ SEI 41-13 for beams and columns. The values in these Tables are adopted in ETABS2016 as default values, therefore; it will be used to model all archetypes mathematically and to model their members nonlinearity. According to section (7.5.3.2) in ASCE/ SEI 41-13, "*Component demands must be within the acceptance criteria for nonlinear components at the selected Structural Performance Level*".

According to part-2 of the commentaries of ASCE/SEI 7-05 and FEMA-450 for design of new buildings, [20, 21], and using the response design spectrum for Baghdad with ordinary and office buildings (category II), the life safety performance level will be aimed, which is the performance objective of most building codes.

## 3. Nonlinear Static Analysis Procedure (NSP)

According to ASCE/ SEI 7– 05, FEMA 450 and ASCE/ SEI 41-13, [4, 22, 13] the gravity load combination for nonlinear analysis in equation 7 will be used and applied before applying the seismic load.

$$W = 1.05D + 0.25L \quad (7)$$

Using ETABS program, the nonlinear designed archetypes shall be subjected into monotonically increasing lateral loads which representing inertia forces in an earthquake till a target displacement (δt) at the control node is exceeded, then the pushover capacity curve will be established.

ETABS2016 will compute the target displacement, using the modified coefficient method of FEMA 440 [23] that adopted in ASCE/SEI 41- 13, to be identified on the pushover curve as the performance point and then to establish the idealized force- displacement curve to get the significant yield point of each nonlinear model.

Gravity loads and P-Δ effects will be included in all analyses. Pushover analyses will be performed by first applying gravity loads, followed by monotonically increasing lateral forces with a specified height-wise distribution.

Based on FEMA 356, the SRSS pattern of lateral force distribution will be used in the NSP analysis, which represents inertia forces in an earthquake. That means, the linear MRS analysis is also performed to supplement the NSP in two ways. The first is to compute the SRSS distribution by back-calculating the lateral forces at each $i^{th}$ floor ($S^*_i$) from the stories shear forces that determined by linear MRS analysis of each model, considering sufficient number of modes to capture a minimum of 90% of the total mass, this will supplement the NSP in case of significant higher mode effects. And secondly; since the NSP analysis required the structure to be designed firstly, it will be designed using the linear MRS analysis considering at least 90% mass participation, this is to compute the earthquake load component to be used in the load combinations for seismic design, and this will verify the adequacy of the design before applying the NSP, which in turn will supplement the NSP analysis to be more trusty. Also, the uniform pattern of lateral force distribution ($S^*_i = m_i$) will be used in the NSP analysis. In addition and Based on ASCE/ SEI 41- 13 and recommendations of FEMA 440, the first mode shape pattern of lateral force distribution will also be used as a third distribution to take into account all possible actions that may occur during actual seismic response, and then the worst case will be the one governing.

## 4. Response Limits and Acceptability Criteria

In this section, the important structural response limits which constitute an acceptance criteria for the archetype structure and adopted in this study, will be summarized as following:

- According to the life safety performance level in ASCE/SEI 41, and Table (12.12.1) in ASCE/SEI 7-05 and Table (4.5.1) in FEMA-450 for ordinary and office buildings (category II), the maximum drift must not exceed 2%. The maximum drift in any one of the nonlinear archetypes is the maximum inter-story drift at the performance point displacement.
- Referring to Table (C1.3) in ASCE/SEI 41, the permanent drift of 1% is indicating the range of inelastic drift that typical structures may undergo when responding within the life safety performance level. The maximum inelastic drift of each of the nonlinear archetypes is defined as the portion of the maximum inter-story drift beyond the effective yield point of the idealized pushover curve [24].
- The ultimate displacement, at which gravity load can no longer be supported and failure occurs, is defined as the roof displacement at a point on the pushover curve of a nonlinear archetype where 20% loss of its maximum strength occurs [4, 8]. The target displacement of a nonlinear archetype represents its performance point or its response to the design earthquake. Thus, the target displacement of a nonlinear archetype need not to exceed its ultimate roof displacement.
- The best collapse mechanism is when the plastic hinges are formed at the ends of beams as much as possible. Then, if the hinges at columns ends are also formed, they are preferred to be in the ground story columns and, their damages are preferred to be just above the foundations. At this stage the collapse mechanism will be

considered to has happened before other hinges at other columns' ends to occur. Thus, the target displacement need to be reached on the pushover curve before the displacement at which the collapse mechanism will be occurred.

- According to ASCE/SEI 41-13 and referring to Figure 4 which represents the generalized load-deformation response for plastic hinges showing the acceptance limit at each performance level, the target displacement need to be reached on the pushover curve of a nonlinear archetype before any hinge response has exceed the acceptance limit at life safety performance level.

## 5. Materials and Methods

Formation of more number of hinges means the stiffness is well distributed, and the seismic forces and then the seismic energy are well distributed along the height which will lead to a more energy dissipation before any one of hinges has reach to failure, and vice versa.

In this section, the overall methodology used for investigating structural behavior will be summarized in the following sequential steps, where for each archetype model and after modeling its joints and supports by ETABS:

- The preliminary columns sections in Table 2 and the preliminary beams sections in Figure 3 are assigned, the effective stiffness of beams ($I_{be}$) will be set to 0.3 of their gross moment of inertia ($0.3I_{bg}$) according to Table 10.5 in ASCE/ SEI 41-13, while the effective stiffness of columns ($I_{ce}$) will preliminarily be set to 0.5 of their gross moment of inertia ($0.5I_{cg}$).
- The nonlinear hinges will be modelled by ETABS based on ASCE/ SEI 41-13, then they are assigned at the two ends of each beam and column.
- Applying the design gravity load combination of equation 1, then the resulting compression ($P_u$) of the outer and inner columns at each story is used to compute the values of ($P_u/A_g f_c'$), then using linear interpolation from Table 10.5 in ASCE/SEI 41-13 to compute the values of $I_{ce}$ at each story, or in other words, $I_{ce} = (P_u / A_g f_c') + 0.2$, which will be reassigned to columns.
- The linear MRS analysis is applied considering a number of modes satisfying at least 90% mass participation, this is to compute the earthquake load component to be used in loads combinations for seismic design.
- Applying the design load combinations of Equations 2c, then the resulting compressions ($P_u$) of the outer and inner columns at the lower of each five stories are used to check whether they are satisfying Equation 6, if they are not, the preliminary sections of columns need to be changed to satisfy Equation 6, and return to Step 2 to reapply Steps 3, 4 and 5 till satisfying Equation 6. It will be seen later that satisfying Equation 6 will keep the column longitudinal reinforcement ratio ($\rho_g$) at the minimum value of 0.01.
- Designing the archetype model according to the design load combinations of Equations 1, 2c and 3c using the program ETABS2016.
- For the worst drift case Steps 3, 4, 5 and 6 will be repeated several times, in each once, the beams depth will be decreased by a step of 5 cm till reaching the depth satisfying two issues; that the longitudinal reinforcement ratios of beams are limited up to the most practical value which is approximately 0.01, and in the same time, to ensure the (SCWB) principle of the ACI 318-14, namely to ensure that ($\Sigma M_{nc}/\Sigma M_{nb} > 1.2$) at the face of each joint, which in turn will ensure that beams will yield before columns or no column yield if ($\Sigma M_{nc}/\Sigma M_{nb}$) is much greater than 1.2 at lower stories. This will promote formation of a better collapse mechanism which is the beam mechanism with much numbers of beams hinges. In most cases, beams sections may need one trial changing.
- When applying the linear MRS analysis as mentioned in Step 3 by considering a number of modes satisfying at least 90% mass participation, the SRSS lateral load distribution will be back- calculated from the shear forces at each floor by copying these shear forces directly from ETABS into a simple MATLAB program and the output will be the SRSS lateral load distribution which will be copied directly into ETABS to be applied at roofs levels.
- Applying the analysis gravity loads combination of Equation 7 and considering the P- Δ effects in ETABS for each nonlinear designed archetype, and then applying the SRSS lateral load distribution by monotonically increasing its lateral forces at roofs along the height till a target displacement ($\delta t$) which will be calculated by ETABS at the control node (the roof of the building), is exceeded, then the pushover capacity curve will be established by ETABS. Also, this step is repeated on another copy of the same nonlinear designed archetype but this time the uniform pattern of lateral force distribution will be applied. Also, this step is again repeated on another copy of the same nonlinear designed archetype but this time the first mode shape pattern of lateral force distribution will be applied.
- Checking items of Section 4 to identify the accepted response limit. The nonlinear structural behavior of the archetype model can be tracked by the part of pushover curve till target displacement (performance point). Also,

the performance point at target displacement represents the maximum response reached by the building through the earthquake. For more clarity, this methodology was represented in Figure 5.

## 6. Results and Discussions

After applying the steps in Section 5 and with reference to steps in Section 4, the columns sections and beams sections for archetypes models in Baghdad have been updated as shown in Table 3 and Figure 6, respectively. Additional archetype models were needed to reach the bound of acceptance limit for each of the three basic configurations, their columns sections are presented in Table 4. The results for the models of each of the three basic configurations are presented and discussed in the following subsections.

### 6.1. Models of the 6 m bay Width Configuration

Figure 7 represents the analysis and design results for archetype model frame of five stories height before applying NSP analysis. Referring to part-c of Figure 7, "It may be reasonable to make an exception to the requirement of ACI 318 regarding strong-column/weak-beam concept at the roof level of a building where a column does not extend above the beam-column joint. At such locations, an interior column may be required to resist moments from two beams in a given framing direction. Columns at such locations commonly support relatively low axial forces, and flexural hinging of the columns at this level will not adversely affect the overall frame mechanism", [3]. Part-b of Figure 7 represents the used columns reinforcement and the required beams reinforcements. Consequently, Figure 8 represents the used reinforcements in beams before applying the NSP. After applying the NSP analysis under the action of the three horizontal load distributions, Figure 9 represents the starting of the formation of the first, second, third and last plastic hinges of columns, (steps 10, 11, 12 and 13), in archetype model frame of five stories height under the action of the 2modes SRSS load distribution pattern. It is clear that all four hinges of columns are formed in the first story during the building response till life safety performance level, although, the columns are weaker than beams at roof level.

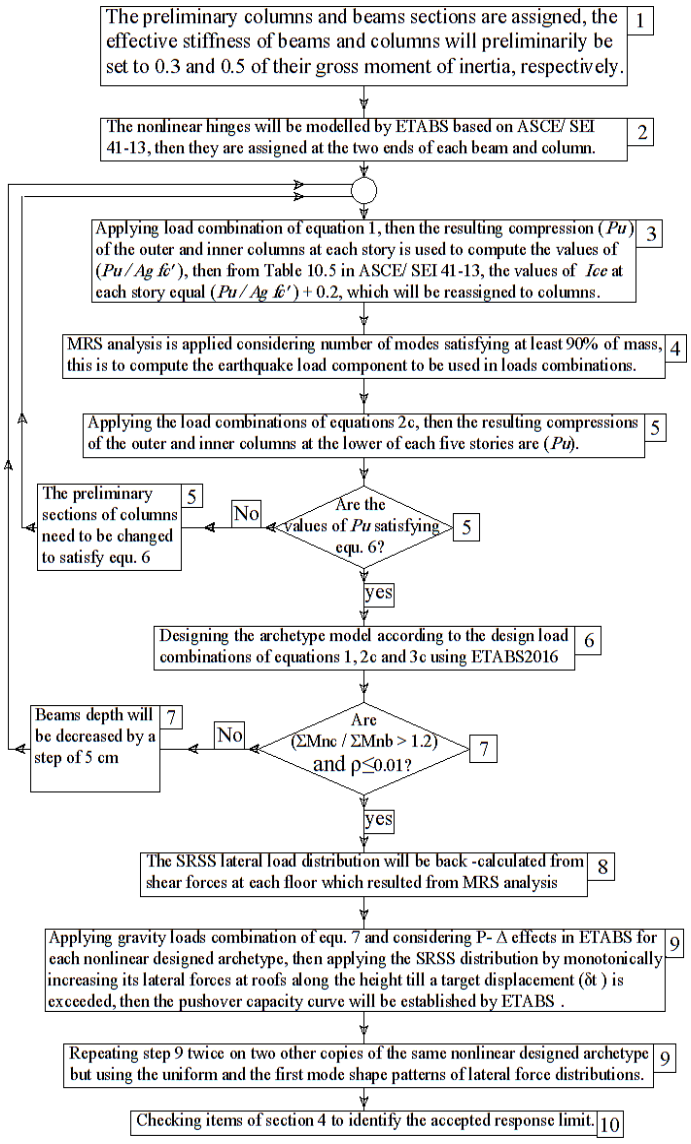


**Figure 5. Flowchart of the used methodology, the number in the square represents the corresponding step number**

**Table 3. Summary of selected column sections after modification**

| Archetypes height steps in terms of number of stories, (*i*) | Column's section depth *h* in meter and values of $f_c'$, *in ksi* [a], *for ;* | | | | | | | |
|---|---|---|---|---|---|---|---|---|
| | 5 stories Model | | 10 stories Model | | 15 stories Model | | 20 stories Model | |
| | h | $f_c'$ | h | $f_c'$ | h | $f_c'$ | h | $f_c'$ |
| **Bay width 6 m** | | | | | | | | |
| 16 to 20 | | | | | | | 0.75 | 5 |
| 11 to 15 | | | | | 0.65 | 5 | 0.75 | 5 |
| 6 to 10 | | | 0.55 | 5 | 0.65 | 5 | 0.75 | 6 |
| 1 to 5 | 0.45 | 5 | 0.55 | 6 | 0.65 | 7 | 0.75 | 7 |
| **Bay width 7.5 m** | | | | | | | | |
| 16 to 20 | | | | | | | 0.95 | 5 |
| 11 to 15 | | | | | 0.85 | 5 | 0.95 | 5 |
| 6 to 10 | | | 0.75 | 5 | 0.85 | 5 | 0.95 | 6 |
| 1 to 5 | 0.60 | 5 | 0.75 | 6 | 0.85 | 7 | 0.95 | 7 |
| **Bay width 9 m** | | | | | | | | |
| 16 to 20 | | | | | | | 1.15 | 5 |
| 11 to 15 | | | | | 1.00 | 5 | 1.15 | 5 |
| 6 to 10 | | | 0.85 | 5 | 1.00 | 5 | 1.15 | 6 |
| 1 to 5 | 0.70 | 5 | 0.85 | 6 | 1.00 | 7 | 1.15 | 7 |

a: 5 ksi = 34.5 MPa, 6 ksi = 41.4 MPa, 7 ksi = 48.3 MPa

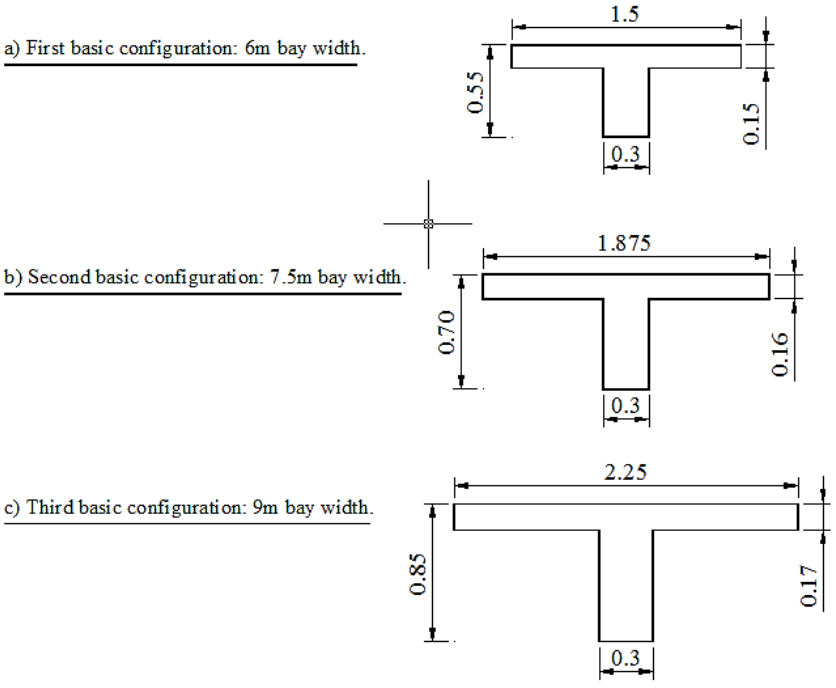


**Figure 6. Modified beams sections for the three basic configurations**

It is worth mentioning here that the target response point of this archetype model frame were reached before starting the plastic hinges yielding in columns, i.e.; before reaching the overall frame failure mechanism. Also, no one of the response limits presented in Section 4 was reached, that means it is need to increase the height till reaching one of them, i.e.; in the other longer archetype models, they may be reached.

In the other archetype model frames and under the action of the three load distribution patterns, it is found that the plastic hinges are also formed only in the archetype model frame of ten stories height during it's response till the life safety performance level. Figures 10 and 11 represent the members sections, longitudinal reinforcement and other responses of the archetype model frame of 6 m bay width and ten stories height. Referring to Figure 10c, and as in the

five stories height model frame, the SCWB requirement at roof level of interior columns is not achieved, and it will be as a reasonable exception as explained previously.

Part-b of Figure 10 represents the used columns reinforcement and the required beams reinforcements. Consequently, Figure 11b represents the used reinforcements in beams and columns before applying the NSP analysis.

Figure 11a represents starting formation of the only plastic hinge in columns (Step 27) since whenever the building height is increased, the required columns sections are increased and then the column/ beam capacity ratios increased to the extent that there will be no plastic hinges formed in the columns, as it was noticed in archetype frame models taller than ten stories height.

**Table 4. Summary of selected column sections for the additional archetype models.**

| Archetypes height steps in terms of number of stories, (*i*) | Column's section depth *h* in meter and values of $f_c'$, *in ksi, for ;* | | | | | | | | | | | |
|---|---|---|---|---|---|---|---|---|---|---|---|---|
| | 17 and 18 stories Models | | 25 stories Model | | 28 stories Model | | 30 stories Model | | 32 stories Model | | 35 stories Model | |
| | h | $f_c'$ | h | $f_c'$ | h | $f_c'$ | h | $f_c'$ | h | $f_c'$ | h | $f_c'$ |
| **Bay width 6 m** | | | | | | | | | | | | |
| 16 to 18 | 0.70 | 5 | | | | | | | | | | |
| 16 to 17,or | 0.70 | 5 | | | | | | | | | | |
| 11 to 15 | 0.70 | 5 | | | | | | | | | | |
| 6 to 10 | 0.70 | 5 | | | | | | | | | | |
| 1 to 5 | 0.70 | 7 | | | | | | | | | | |
| **Bay width 7.5 m** | | | | | | | | | | | | |
| 26 to 28 | | | | | 1.10 | 5 | | | | | | |
| 21 to 25 | | | 1.05 | 5 | 1.10 | 5 | | | | | | |
| 16 to 20 | | | 1.05 | 5 | 1.10 | 5 | | | | | | |
| 11 to 15 | | | 1.05 | 5 | 1.10 | 5 | | | | | | |
| 6 to 10 | | | 1.05 | 6 | 1.10 | 6 | | | | | | |
| 1 to 5 | | | 1.05 | 7 | 1.10 | 7 | | | | | | |
| **Bay width 9 m** | | | | | | | | | | | | |
| 33 to 35 | | | | | | | | | | | 1.45 | 5 |
| 31 to 32 | | | | | | | | | 1.40 | 5 | 1.45 | 5 |
| 26 to 30 | | | | | | | 1.35 | 5 | 1.40 | 5 | 1.45 | 5 |
| 21 to 25 | | | 1.25 | 5 | | | 1.35 | 5 | 1.40 | 5 | 1.45 | 5 |
| 16 to 20 | | | 1.25 | 5 | | | 1.35 | 5 | 1.40 | 5 | 1.45 | 5 |
| 11 to 15 | | | 1.25 | 5 | | | 1.35 | 5 | 1.40 | 5 | 1.45 | 5 |
| 6 to 10 | | | 1.25 | 6 | | | 1.35 | 6 | 1.40 | 6 | 1.45 | 6 |
| 1 to 5 | | | 1.25 | 7 | | | 1.35 | 7 | 1.40 | 7 | 1.45 | 7 |


**Figure 7. Archetype model frame of 6 m bay width and five stories height; a) Members sections, b) longitudinal reinforcement, c) column / beam capacity Ratios**

Beam Name: T *h* - *SNs* To *SNe* - *SP* , where;

T: Beam section type (Tee Beam),
*h*: Depth of section, [mm],
Beams of this section type are used in storeys from storey number *SNs* to storey number *SNe*,
*SP*: Span designation, where A, B and C meaning the first, middle and end spans, respectively.

Column Name: C *h* - *SNs* To *SNe* - *fc'* , where;

C: Column section type (square with reinforcement equally distributed on four faces),
*h*: Depth of section, [mm],
Columns of this section type are used in stories from story number *SNs* to story number *SNe*,
*fc'*: concrete compressive strength in [ksi].

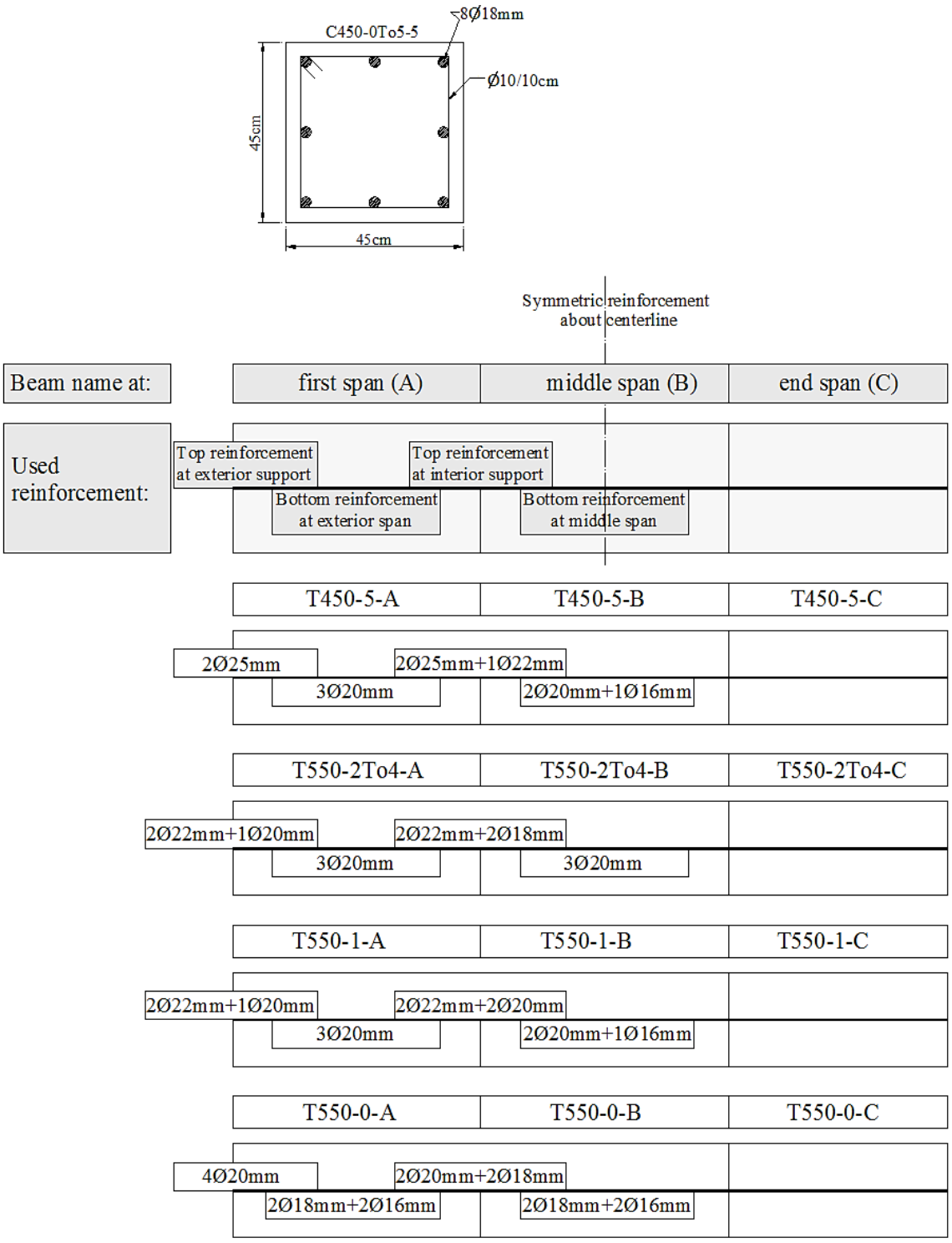


**Figure 8. The used reinforcements in columns and beams of archetype model frame of five stories height and the designation used to define their names in Figure 6**

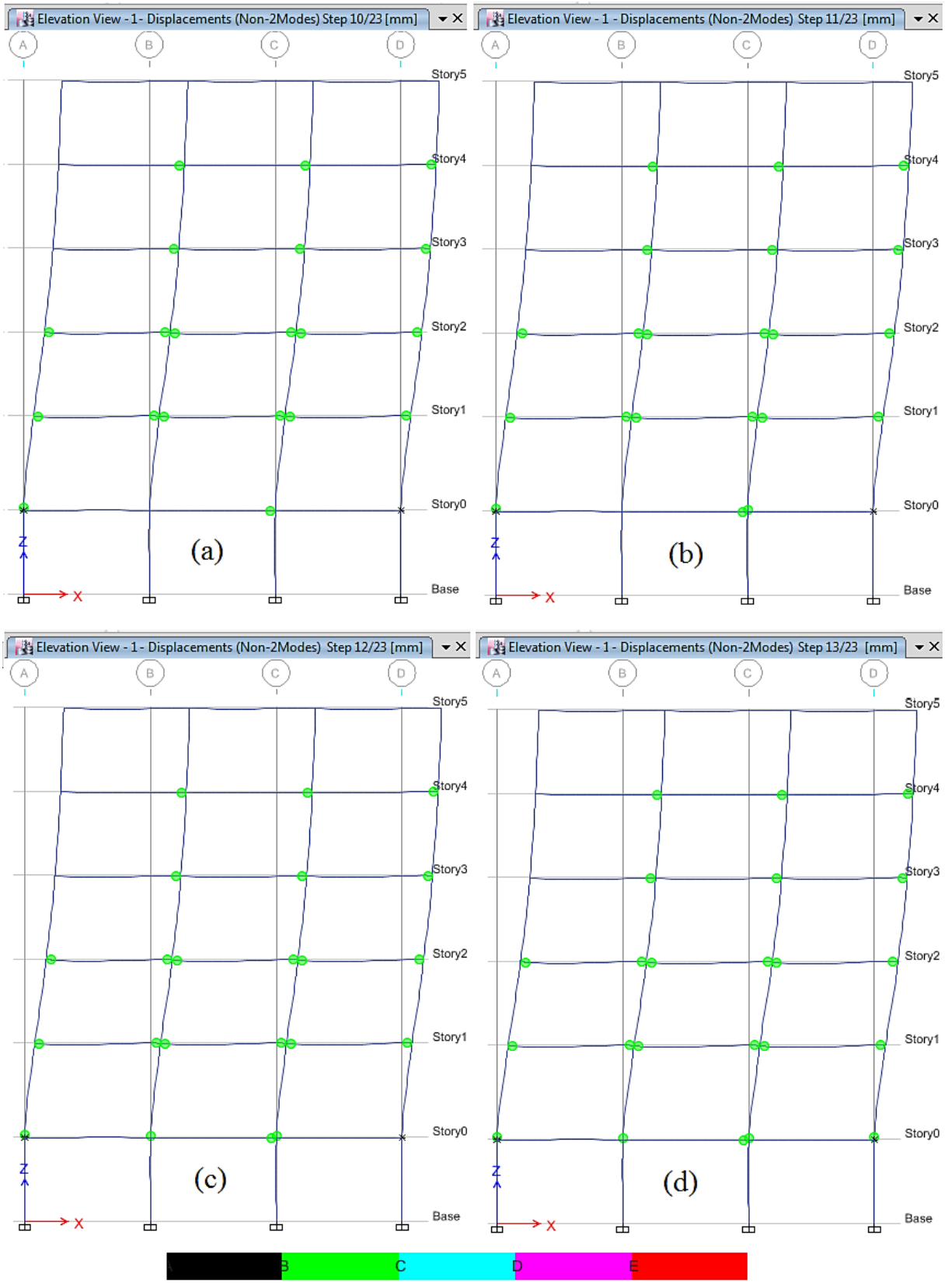


**Figure 9. Plastic hinges formation in archetype model frame of 6m bay width and five stories height. Formation of the; a) first hinge of columns started, b) second hinge of columns started, c) third hinge of columns started; and d) last hinge of columns started**

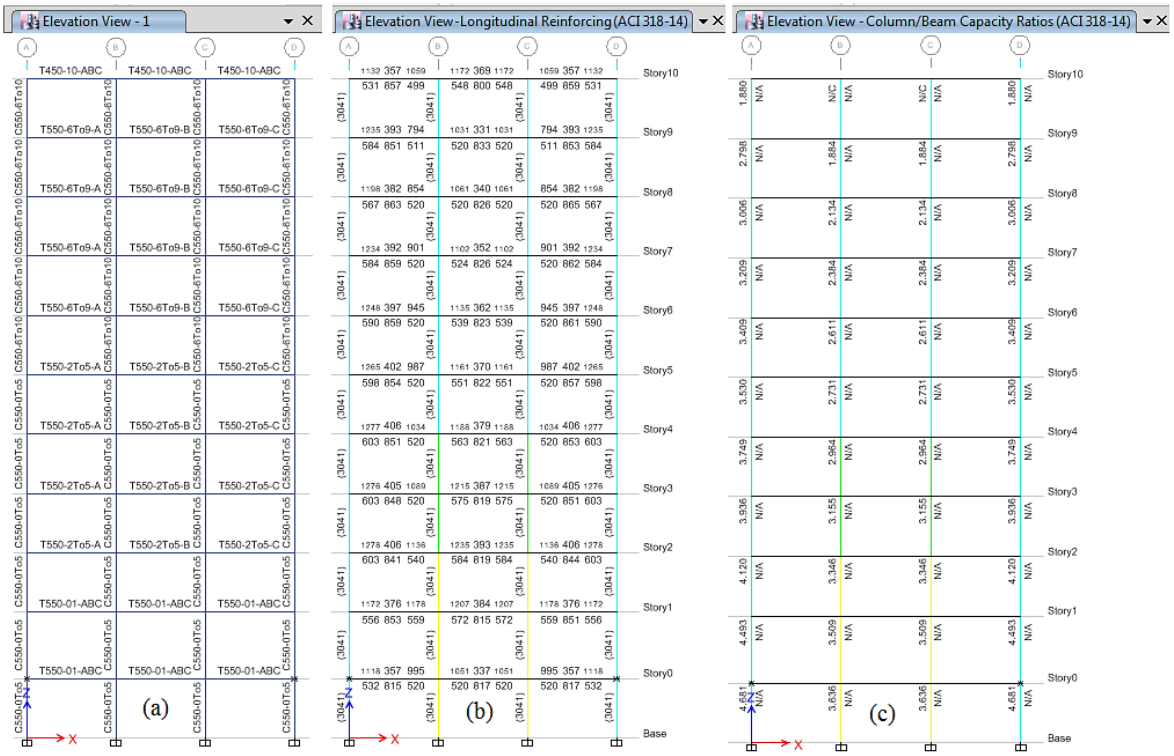


**Figure 10. Archetype model frame of 6m bay width and ten stories height; a) Members sections, b) longitudinal reinforcement, c) column / beam capacity Ratios**

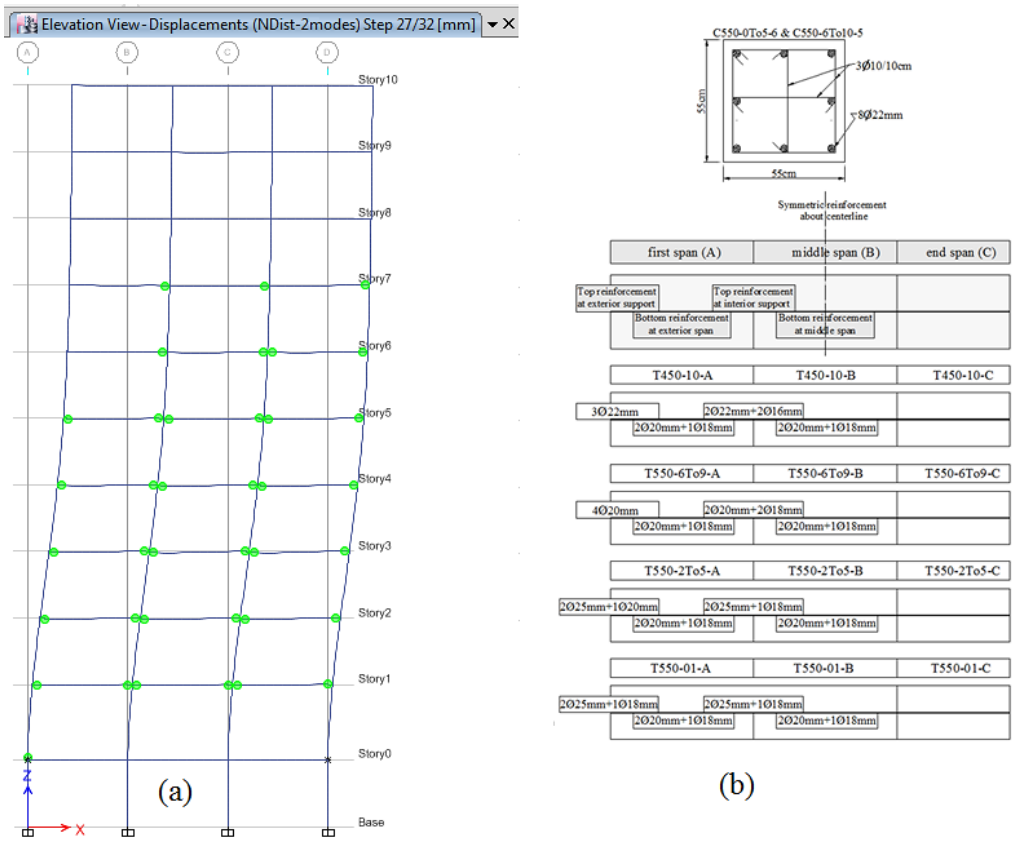


**Figure 11. Archetype model frame of 6m bay width and ten stories height; a) formation of the only plastic hinge of columns started, b) the used reinforcements in columns and beams**

Figures 12, 13 and 14 represent the pushover curves for archetype model frame of five stories height under the action of the 1st Mode, SRSS of first two modes and uniform load distribution patterns, respectively. The inter-story inelastic or plastic drift ratio ($IDR_p$) is the difference between the inter-story drift ratios at target displacement ($\delta_t$) and that at the effective yield displacement ($D_y$), ($IDR_t$ and $IDR_y$), both at a specified story, [24]. The maximum inter-story

plastic drift ratio ($IDR_{pmax}$) is the maximum $IDR_p$ of all stories, or in accurate words it is the difference at a specified story where maximum difference is, in this case, $IDR_t$ and $IDR_y$ will be designated as $IDR_{tmax}$ and $IDR_{ymax}$. Both, $\delta_t$ and $D_y$ are taken from the output

Plate of each pushover curve. Each NSP analysis includes a number of loading steps to draw the pushover curve. To identify the two steps at which $\delta_t$ and $D_y$ are reached, the deformed archetype shape, like those in Figure 8, is pushed to reach the values of $D_y$ and $\delta_t$ at roof level, this is for each NSP analysis of each load distribution pattern. After identifying the step number to reach $D_y$ and that to reach $\delta_t$, from the stories drift distribution plot along the height at the identified two steps for δt and Dy, the value and the story at which the maximum difference, between the stories drift ratios in these two steps, can be determined. In most cases, $\delta_t$ and $D_y$ are not identified at exact steps, but, between two steps which are previous and next steps, therefore, linear interpolation need to be applied.

From Figure 12, $\delta_t$ = 146.395 mm and $D_y$ = 60.615 mm. Figure 15 represents the deformed shape at the two pairs of steps before and after reaching $D_y$ and $\delta_t$ at roof level which are Steps 2, 3, 5 and 6 respectively, this is from the NSP analysis of the archetype model frame of five stories height under the action of the 1st Mode load distribution. At these steps, the roof displacements are 47, 80.8, 143.2 and 147.2 mm, respectively.

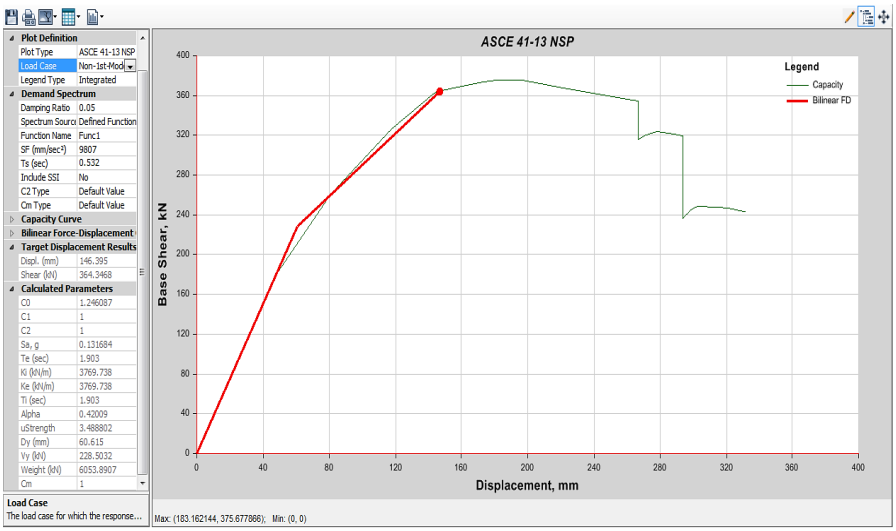


**Figure 12. Pushover curve for archetype model frame of 6m bay width and five stories height under the action of the 1st-Mode horizontal load distribution pattern**

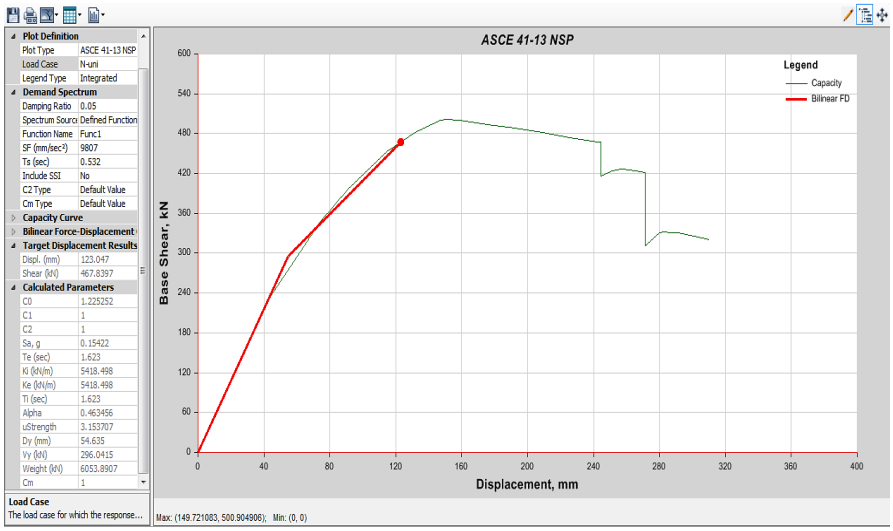


**Figure 13. Pushover curve for archetype model frame of 6m bay width and five stories height under the action of the SRSS horizontal load distribution from the first two modes**

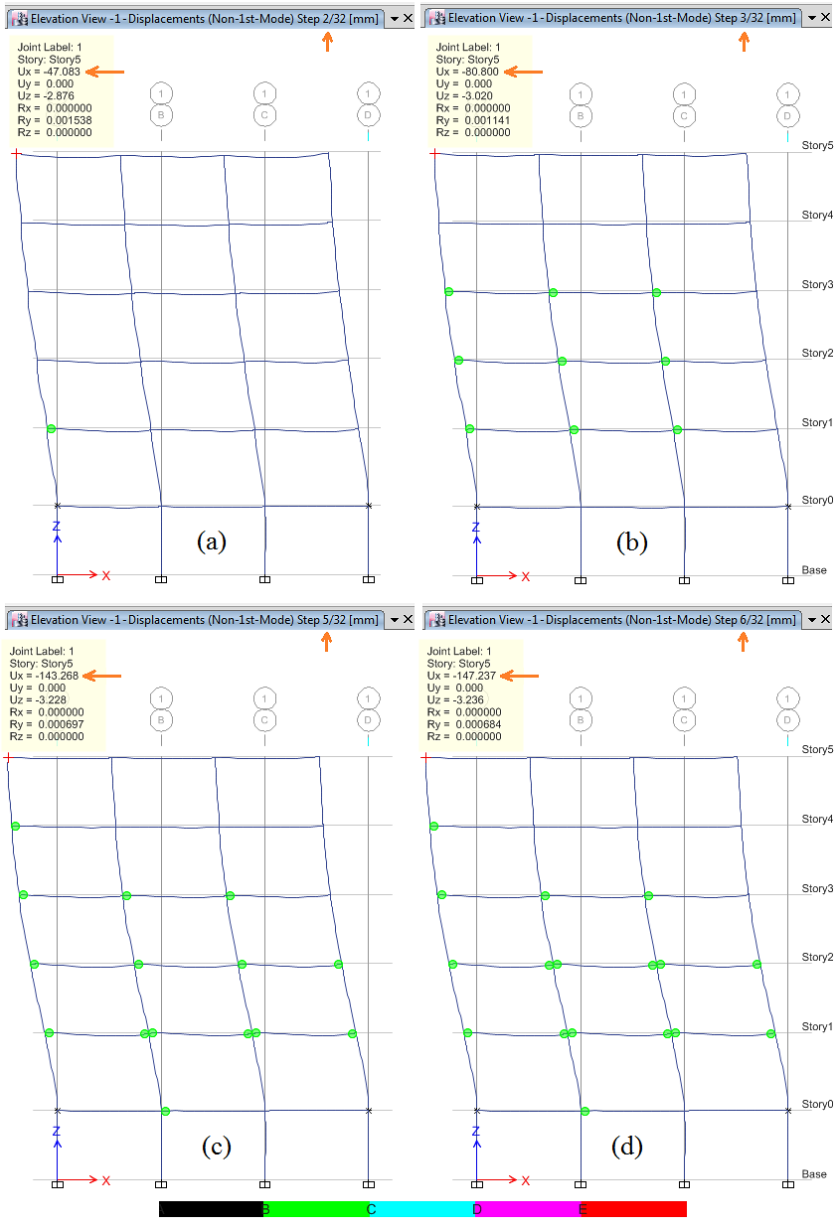


**Figure 14. Pushover curve for archetype model frame of 6m bay width and five stories height under the action of the uniform horizontal load distribution pattern**

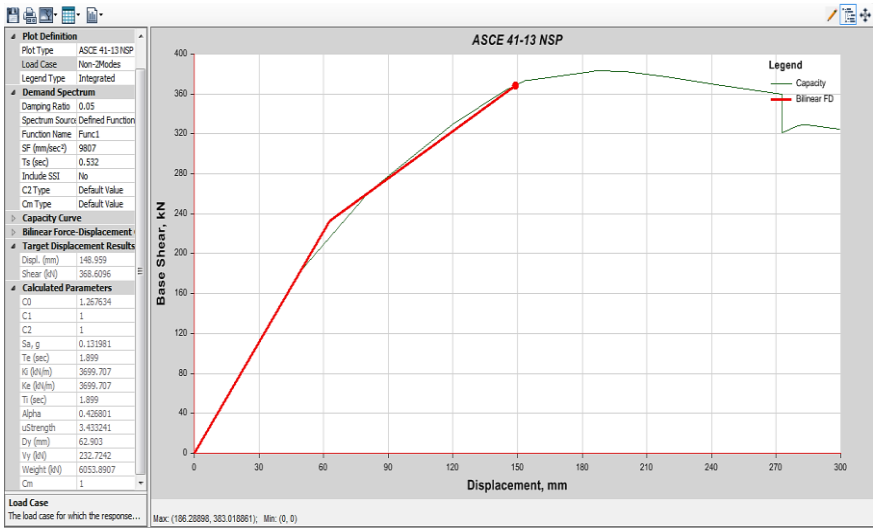


**Figure 15. Deformed shape for archetype model frame of 6m bay width and five stories height resulted from the NSP of the1st-Mode load pattern at steps directly: a) before $D_y$, step-2, b) after $D_y$, step-3, c) before $\delta_t$, step-5, and; d) after $\delta_t$, step 6**

Figure 16a, b, c and d represents the inter- story drift ratios along the height of archetype model frame of 6 m bay width and five stories height resulted from the NSP of the 1st-Mode load pattern at steps directly before and after reaching $D_y$, Steps 2 and 3, and at steps directly before and after reaching $\delta_t$, Steps 5 and 6, respectively, and it can be extrapolated from this Figure that the maximum difference in drift ratios will be at Story 2, therefore; the drift ratios at Story 2 in Steps 2, 3, 5 and 6 are determined from Parts a, b, c and d of the same Figure, which Equal 0.002943, 0.005555, 0.010279 and 0.010631, respectively. Now, after getting the roof displacements and drift ratios at Story 2 corresponding to the Steps that are immediately before and after $D_y$ and $\delta_t$, (i.e.; steps 2, 3, 5 and 6), the maximum inelastic drift ratio will be at Story 2 and will be calculated by linear interpolation between values in Steps 2 and 3 to determine the $IDR_{ymax}$ corresponding to $D_y$, and between values in Steps 5 and 6 to determine the $IDR_{tmax}$ corresponding to $\delta_t$. Then, the difference between these two values of IDR will be the maximum inelastic drift ratio ($IDR_{pmax}$), as shown schematically in Figures 17 and 18 for three NSP analyses corresponding to the three adopted load distribution patterns.

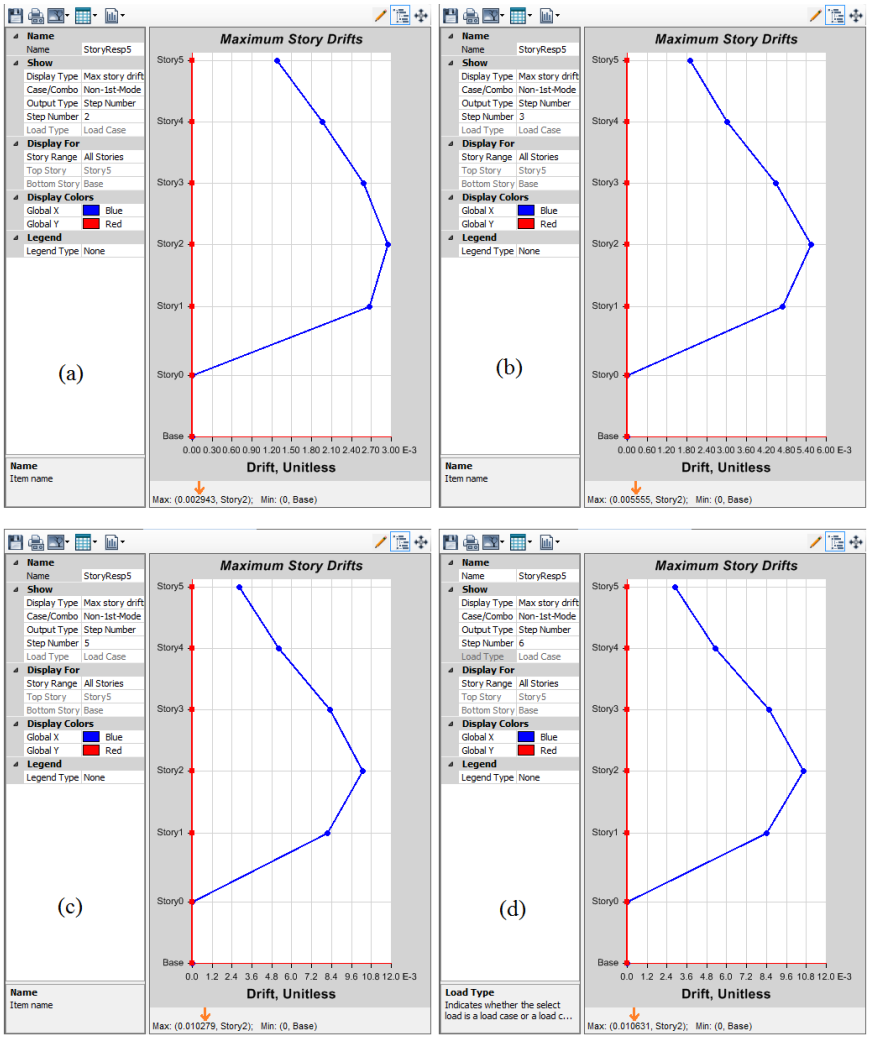


**Figure 16. Inter-story drift ratios (IDR) along the height of archetype model frame of 6m bay width and five stories height**

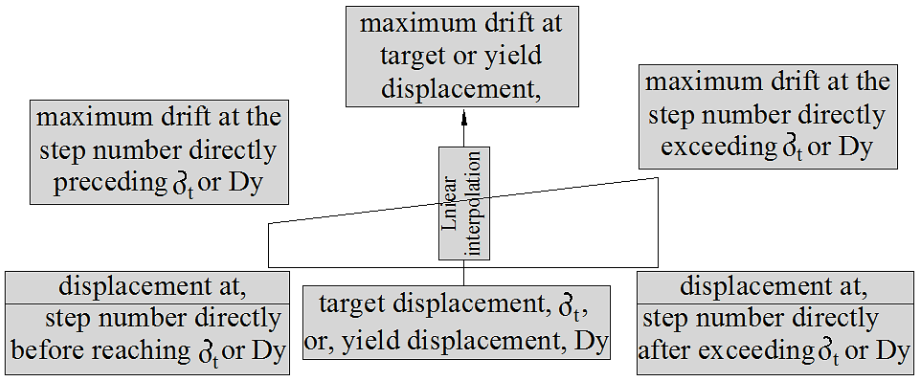


**Figure 17. Schematic sketch for the designation of items and their locations in the interpolation used to calculate the maximum inter-story drift ratios at target and effective yield displacements**

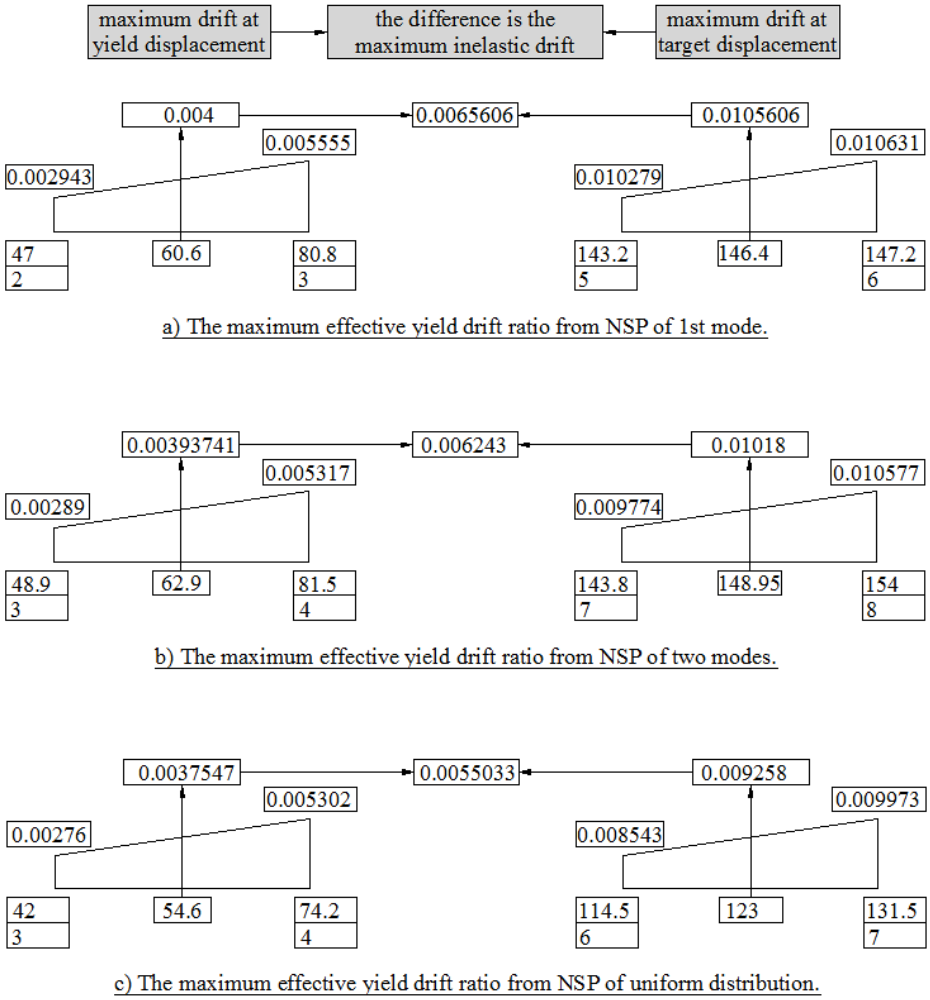


**Figure 18. Schematic sketches for the calculation of the maximum inter-story inelastic drift ratio (IDRpmax) from; a) the NSP of the 1st mode load distribution, b) the NSP of the two- modes load distribution, c) the NSP of the uniform load distribution of archetype model frame of 6m bay width and five stories height**

Table 5 represents the $IDR_{pmax}$ computed values for the 5, 10, 15 and 20 stories heights frame models under the action of the three load distributions, and also for the additional 17 and 18 stories heights frame models.

The values of $IDR_{pmax}$ are plotted against height of frame models in Figure 19. It can be seen that the slope of the two lines from the 1st- mode and the multi- mode load distributions clearly decreases at the frame models of 17 story height and taller with more increase in plastic drift, while this is not appear clearly in the line of the uniform load distribution. Also, the plastic drift ratios in cases of 1st – mode and multi- mode load patterns exceed the limit of 1% of item- 2 in Section 4. But, the maximum inter-story drift ratios at $\delta_t$ ($IDR_{tmax}$) do not exceed the limit of 2% of item- 1 in Section 4.

**Table 5. IDRpmax computed values for the 6m bay width and 5, 10, 15, 17, 18 and 20 stories heights frame models under the action of the three load distributions**

| Height in terms of number of stories | Inter- story drift ratios x $10^{-2}$ | | | | | | | | |
|---|---|---|---|---|---|---|---|---|---|
| | 1st mode load distribution | | | Multi-mode load distribution | | | Uniform load distribution | | |
| | $IDR_{tmax}$ at $\delta t$ | $IDR_{ymax}$ at $D_y$ | $IDR_{pmax}$ | $IDR_{tmax}$ at $\delta t$ | $IDR_{ymax}$ at $D_y$ | $IDR_{pmax}$ | $IDR_{tmax}$ at $\delta t$ | $IDR_{ymax}$ at $D_y$ | $IDR_{pmax}$ |
| 20 | 1.441 | --- | --- | 1.4053 | 0.3498 | 1.0555 | 1.29 | 0.3401 | 0.9499 |
| 18 | 1.385 | 0.346 | 1.039 | 1.352 | 0.351 | 1.001 | 1.275 | 0.347 | 0.928 |
| 17 | 1.335 | 0.343 | 0.992 | 1.295 | 0.3477 | 0.9473 | 1.2303 | 0.3463 | 0.884 |
| 15 | 1.284 | 0.351 | 0.933 | 1.246 | 0.355 | 0.891 | 1.162 | 0.3478 | 0.8142 |
| 10 | 1.155 | 0.386 | 0.769 | 1.122 | 0.388 | 0.734 | 1.044 | 0.398 | 0.646 |
| 5 | 1.05606 | 0.4 | 0.65606 | 1.018 | 0.3937 | 0.6243 | 0.9258 | 0.37547 | 0.55033 |

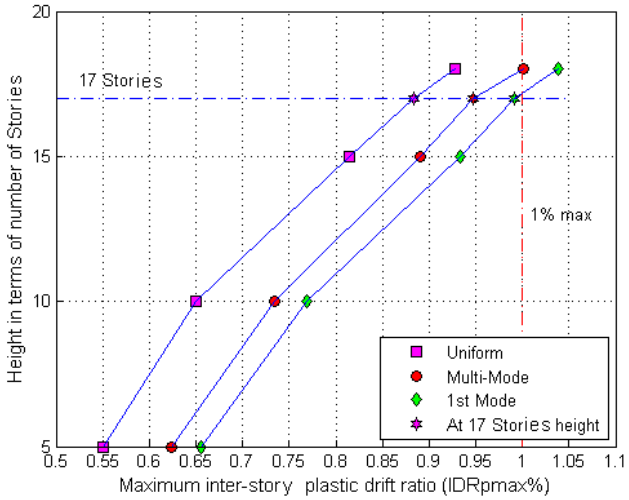


**Figure 19. IDRpmax computed values for the 6m bay width and 5, 10, 15, 17, 18 and 20 stories heights frame models under the action of the three load distributions**

Figures 20, 21 and 22 represent the pushover curves for archetype model frame of ten stories height under the action of the 1st Mode, SRSS of first two modes and uniform load distribution patterns, respectively.

Also, Figures 23, 24 and 25 represent the pushover curves for archetype model frame of fifteen stories height under the action of the 1st Mode, SRSS of first two modes and uniform load distribution patterns, respectively.

From these six Figures and their output plates, it can be noticed that the post-yield slope (α) started to become negative in archetype frame model of 15 stories height, and it will be increased in negative in archetype frame models taller than 15 stories height. (α: called "Alpha" in output plate of pushover curve). Besides that, the target displacement ($\delta_t$) increases and, conversely, the target shear (shear capacity, $V_t$) decreases, to be both clearly located on the descending part of the curve where the ultimate point of displacement ($\delta_u$) and the corresponding minimum shear ($V_{min}$) will be. In this case, it is need to check whether the target displacement still within the ultimate one or not, or in other word, it is need to check whether the shear capacity ($V_t$) still higher than $V_{min}$ or not.

The ultimate point of displacement is located at 20% loss of the maximum shear ($V_{max}$) on the right descending part of the pushover capacity curve. In mathematical words, it is need to check whether $V_t$, on the the right descending part of the pushover capacity curve, still higher than $V_{min} = 0.8V_{max}$ or not. The target shear ($V_t$) is directly taken from the output plate of the pushover curve while $V_{max}$ is determined on the curve, or in fact will be written down the curve as a "max and min" values, as clear in all previously mentioned Figures of pushover curves. For more clarity, and in reference to Figure 23, $V_t$ = 251.13 kN, $V_{max}$ = 283.23 kN, from which $V_{min}$ = 226.6 kN, therefore, the shear capacity ($V_t$) still higher than $V_{min}$.

Table 6 represents the $V_t$, $V_{max}$ and $V_{min}$ values for the 15 and 20 stories heights frame models under the action of the three load distributions, and also for the additional 17 and 18 stories heights frame models. The target shear capacity ($V_t$) and the minimum shear capacity ($V_{min}$) are plotted, against the heights of the 6m bay width archetype frame models for the three load distributions, in Figure 26. Several notes can be concluded from Figure 26, first of all, the smallest target shear capacity and the larger target displacement demand are under the effect of the 1st- mode load distribution pattern, which is the worst case among the three load distributions. Also, as the building height increased, both, the target and the minimum shear capacities decrease and the target displacement increases under the effect of the same earthquake ground motion, this due to the increased P-delta effects.

But the rate of decrease in target shear is more than that in the minimum shear, and it continues more with height until the target shear capacity becomes equal to and, then less than, the minimum shear capacity for the 1st- mode load distribution and then the multi- mode load distribution, this is between stories 17 and 18, while this will be near 20 stories under the effect of the uniform load distribution. For this reason, the slope of lines in Figure 19 clearly decreases after story 17 and with highly increase in plastic drift under the effect of the two load distributions, the 1st- mode and the multi- mode. While for the line of the uniform load, this behavior does not appear obvious on it. Anyway, and for the previous reasons which meet item 3 in Section 4, the 17 stories height will be considered as the maximum limit for the building frames of 6 m bay width.

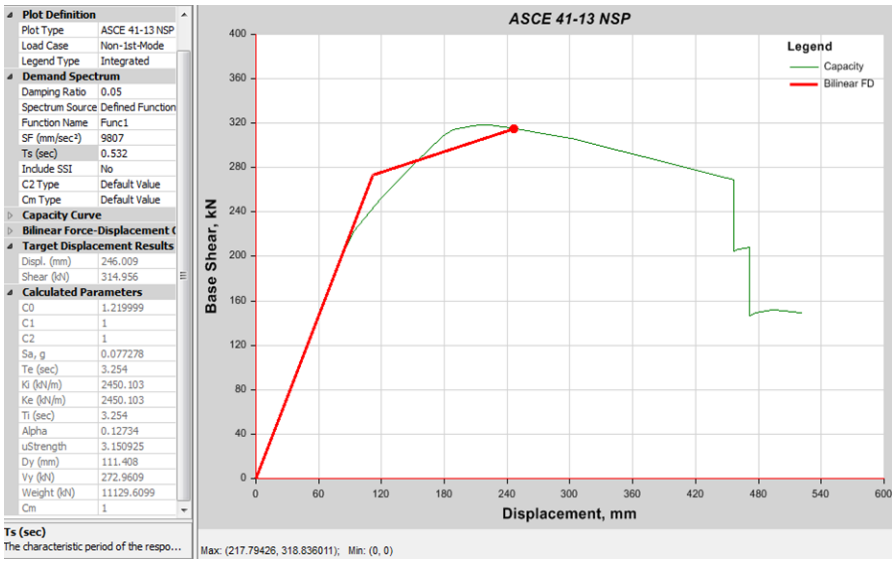


**Figure 20. Pushover curve for archetype model frame of 6 m bay width and ten stories height under the action of the 1st-Mode horizontal load distribution pattern**

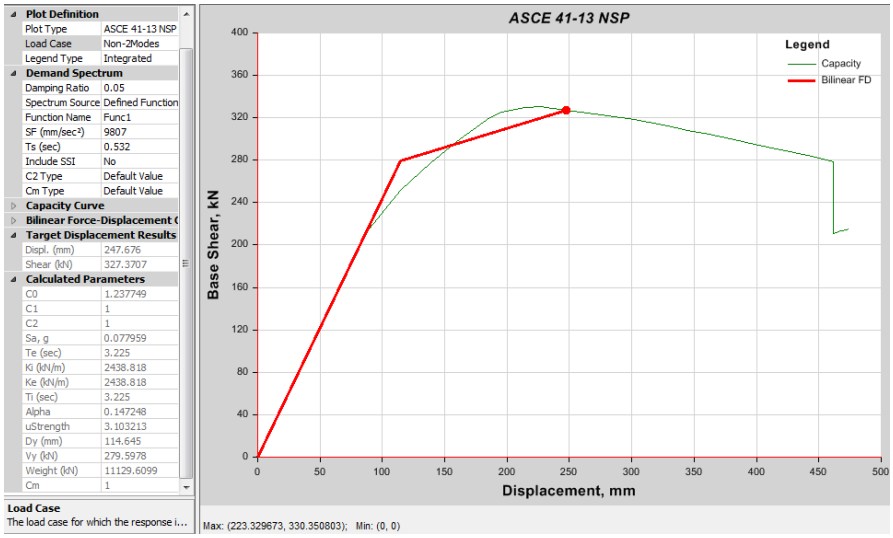


**Figure 21. Pushover curve for archetype model frame of 6 m bay width and ten stories height under the action of the SRSS horizontal load distribution from the first two modes**

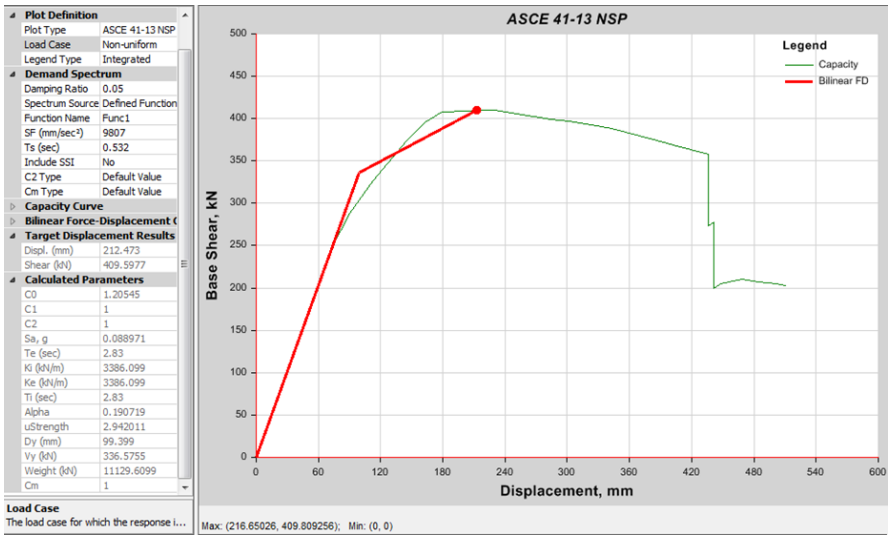


**Figure 22. Pushover curve for archetype model frame of 6m bay width and ten stories height under the action of the uniform horizontal load distribution pattern**

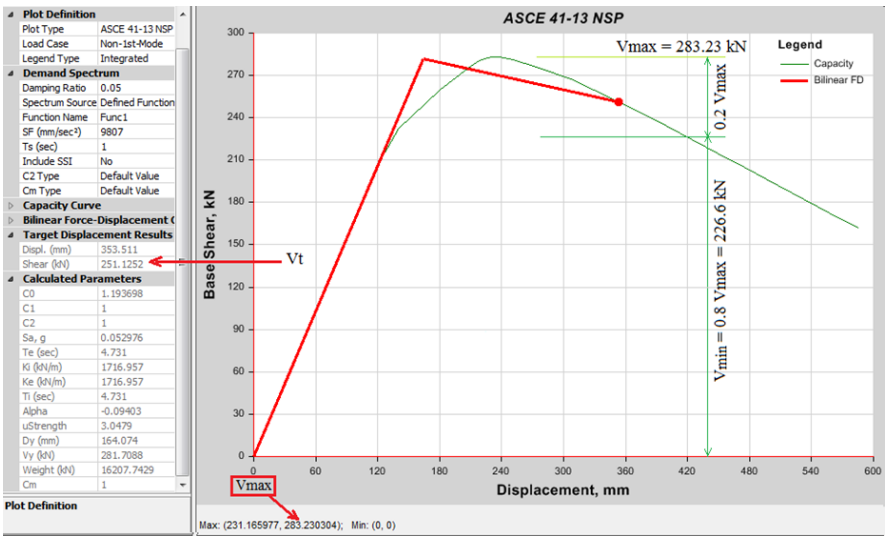


**Figure 23. Pushover curve for archetype model frame of 6 m bay width and fifteen stories height under the action of the 1st-Mode horizontal load distribution pattern**

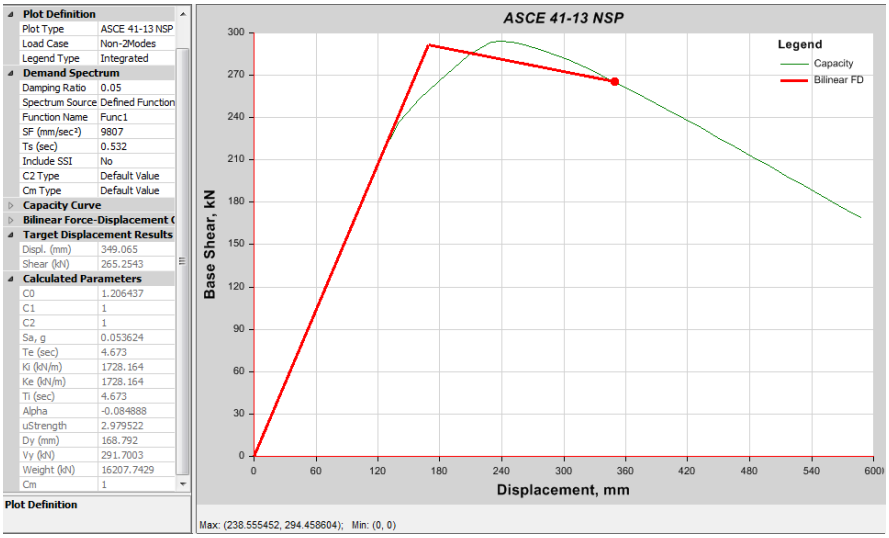


**Figure 24. Pushover curve for archetype model frame of 6 m bay width and fifteen stories height under the action of the SRSS horizontal load distribution from the first two modes**

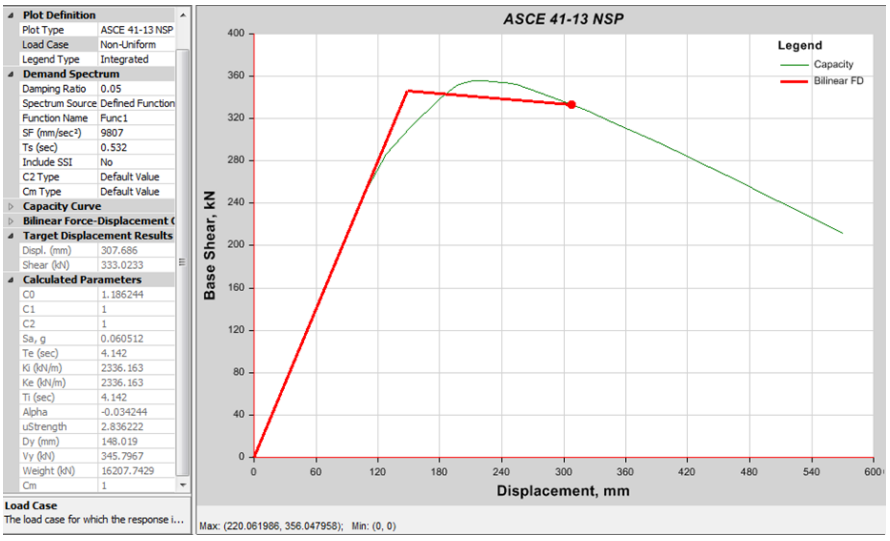


**Figure 25. Pushover curve for archetype model frame of 6 m bay width and fifteen stories height under the action of the uniform horizontal load distribution pattern**

**Table 6. The target, maximum and minimum shear values (Vt, Vmax and Vmin) for the 6m bay width and 15, 17, 18 and 20 stories heights frame models under the action of the three load distributions**

| Height in terms of number of stories | Shear values in (kN) | | | | | | | | |
|---|---|---|---|---|---|---|---|---|---|
| | 1st mode load distribution | | | Multi-mode load distribution | | | Uniform load distribution | | |
| | Vt | Vmax | Vmin | Vt | Vmax | Vmin | Vt | Vmax | Vmin |
| 20 | 175 | 253 | 202.4 | 189.24 | 266.5 | 213.2 | 246.44 | 315 | 252 |
| 18 | 200.8 | 259 | 207.2 | 216.6 | 273 | 218.4 | 274.7 | 324 | 259.2 |
| 17 | 223.43 | 274.37 | 219.5 | 240.6 | 284 | 227.2 | 301 | 337.5 | 270 |
| 15 | 251 | 283.23 | 226.6 | 265.3 | 294.5 | 235.6 | 333 | 356 | 284.8 |

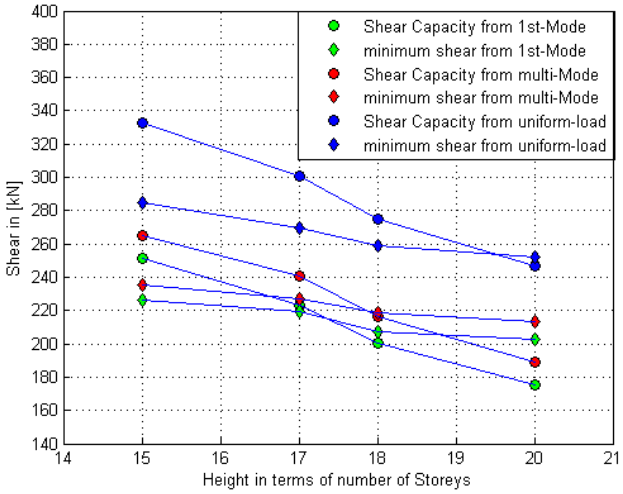


**Figure 26. The shear capacity and minimum shear against the height of the 6m bay width and 15, 17, 18 and 20 stories heights frame models under the action of the three load distributions**

## 6.2. Models of the 7.5 m bay Width Configuration

Table 7 represents the values of $IDR_{t\ max}$ and $IDR_{ymax}$ from which $IDR_{pmax}$ is computed for the 5, 10, 15 and 20 stories heights frame models under the action of the three load distributions, and also for the additional 25, 27, 28 and 30 stories heights frame models. The maximum inter-story plastic drift ratio ($IDR_{pmax}$) is also plotted in Figure 27 against heights of the 7.5m bay width archetype frame models for the three load distributions.

**Table 7. IDRpmax computed values for the 7.5 m bay width and 5, 10, 15, 20, 25, 27, 28 and 30 stories heights frame models under the action of the three load distributions**

| Height in terms of number of stories | Inter- story drift ratios x $10^{-2}$ | | | | | | | | |
|---|---|---|---|---|---|---|---|---|---|
| | 1st mode load distribution | | | Multi-mode load distribution | | | Uniform load distribution | | |
| | $IDR_{tmax}$ at δt | $IDR_{ymax}$ at $D_y$ | $IDR_{pmax}$ | $IDR_{tmax}$ at δt | $IDR_{ymax}$ at $D_y$ | $IDR_{pmax}$ | $IDR_{tmax}$ at δt | $IDR_{ymax}$ at $D_y$ | $IDR_{pmax}$ |
| 30 | 1.310 | 0.378 | 0.932 | 1.258 | 0.3767 | 0.8813 | 1.1702 | 0.37757 | 0.7926 |
| 28 | 1.267 | 0.3868 | 0.8802 | 1.21 | 0.3855 | 0.8245 | 1.14 | 0.37727 | 0.7627 |
| 27 | 1.226 | 0.3774 | 0.8486 | 1.177 | 0.3751 | 0.8019 | 1.11 | 0.365 | 0.745 |
| 25 | 1.185 | 0.3756 | 0.8094 | 1.145 | 0.3783 | 0.7667 | 1.088 | 0.37337 | 0.7146 |
| 20 | 1.076 | 0.359 | 0.717 | 1.041 | 0.370 | 0.671 | 0.995 | 0.3736 | 0.6214 |
| 15 | 0.9732 | 0.3651 | 0.6081 | 0.9272 | 0.3696 | 0.5576 | 0.902 | 0.3684 | 0.5336 |
| 10 | 0.9178 | 0.3517 | 0.5661 | 0.864 | 0.3489 | 0.5151 | 0.8368 | 0.3335 | 0.5033 |
| 5 | 0.8523 | 0.291 | 0.56133 | 0.8193 | 0.307 | 0.5123 | 0.755 | 0.2868 | 0.4682 |

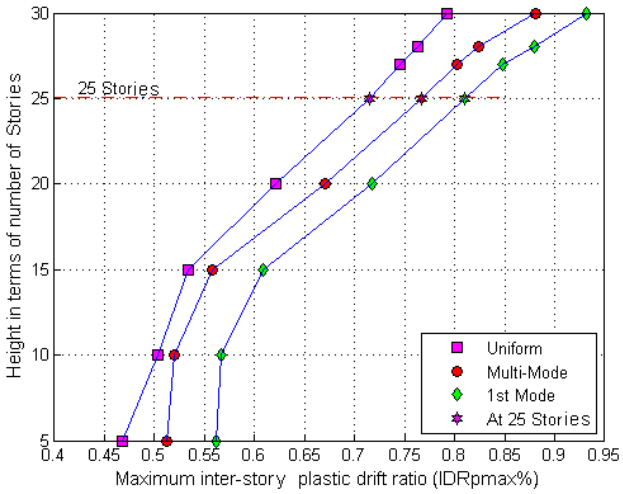


**Figure 27. IDRpmax computed values for the 7.5 m bay width and 5, 10, 15, 20, 25, 27, 28 and 30 stories heights frame models under the action of the three load distributions**

It can be seen that the slope of the line from the 1st- mode load distribution clearly decreases at frame model of 27 story height and taller with more increase in plastic drift, and the line from the multi- mode load distribution will clearly decrease at frame model of 28 story height and taller with more increase in plastic drift, while this is not appear clearly in the line of the uniform load distribution. But, the plastic drift ratios do not exceed the limit of 1% of item 2 in section 4. Also from Table 7, the maximum inter-story drift ratios at $\delta_t$ ($IDR_{tmax}$) do not exceed the limit of 2% of item 1 in Section 4. The behavior of the plastic drifts from the three load distributions will be interpreted basing on the shear capacities, as follows.

Table 8 represents the values of the $V_t$, $V_{max}$ and $V_{min}$ for the 20 stories height frame model under the action of the three load distributions, and also for the additional 25, 27, 28 and 30 stories heights frame models. The target shear capacity ($V_t$) and the minimum shear capacity ($V_{min}$) were plotted, against the heights of the 7.5 m bay width archetype frame models for the three load distributions, in Figure 28. Same notes in archetype models of 6m bay width can be concluded here from Figure 27 and Table 8, first of all, the smallest target shear capacity and the larger target displacement demand are under the effect of the 1st- mode load distribution pattern, which is the worst case among the three load distributions. Also, as the building height increased, both, the target and the minimum shear capacities decrease and the target displacement increases under the effect of the same earthquake ground motion, this due to the increased P-delta effects in taller (i.e.; heavier ) buildings. But the rate of decrease in target shear is more than that in the minimum shear, and it continues more with height until the target shear capacity becomes equal to and, then less than, the minimum shear capacity.

In the 1st- mode load distribution, the target shear capacity ($V_t$) is the first among those in the other load distributions, reaches, and then be less than, the corresponding minimum shear capacity ($V_{min}$) at an archetype model height slightly lower than 27 stories. In the multi- mode load distribution, the $V_t$ reaches, and then be less than, the corresponding $V_{min}$ at an archetype model height lower than and near 28 stories, while in the uniform load distribution, it reaches, and then be less than, the corresponding $V_{min}$ at an archetype model height lower than and near 30 stories, which is the last model. That is why in Figure 27, the slope of the lines of $IDR_{pmax}$ from the 1st- mode and multi- mode load distributions clearly decreases at, and taller than, frame model heights of 27 and 28 stories heights, respectively, with highly increase in plastic drifts, while for the line of the uniform load, this behavior does not appear obvious on it because it's $V_t$ started to be less than the corresponding $V_{min}$ near the last model. Anyway, and for the previous reasons which meet item- 3 in section 4, the 25 stories height will be considered as the maximum limit for the building frames of 7.5 m bay width.

**Table 8. The target, maximum and minimum shear values (Vt, Vmax and Vmin) for the 7.5m bay width and 20, 25, 27, 28 and 30 stories heights frame models under the action of the three load distributions**

| Height in terms of number of stories | Shear values in (kN) | | | | | | | | |
|---|---|---|---|---|---|---|---|---|---|
| | 1st mode load distribution | | | Multi-mode load distribution | | | Uniform load distribution | | |
| | Vt | Vmax | Vmin | Vt | Vmax | Vmin | Vt | Vmax | Vmin |
| 30 | 310.1 | 451.6 | 361.28 | 344.4 | 480.3 | 384.24 | 449.8 | 570.9 | 456.72 |
| 28 | 357.7 | 473.3 | 378.64 | 396.4 | 503.4 | 402.72 | 502.6 | 599.8 | 479.84 |
| 27 | 383.8 | 481.13 | 384.9 | 419.7 | 510.6 | 408.48 | 531.12 | 609.6 | 487.68 |
| 25 | 421.9 | 507.5 | 406.0 | 458.5 | 527.6 | 422.08 | 572.4 | 630.3 | 504.24 |
| 20 | 520.7 | 547.3 | 437.84 | 555.7 | 578.7 | 462.96 | 685.03 | 698.4 | 558.72 |

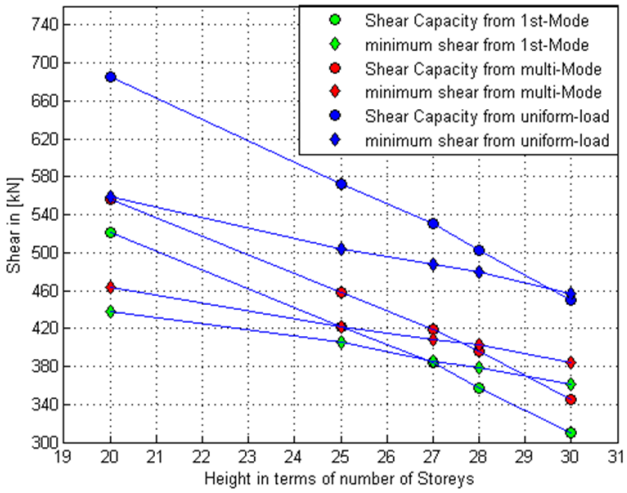


**Figure 28. The shear capacity and minimum shear against the height of the 7.5m bay width and 20, 25, 27, 28 and 30 stories heights frame models under the action of the three load distributions.**

## 6.3. Models of the 9 m bay Width Configuration

Table 9 represents the values of $IDR_{t\ max}$ and $IDR_{ymax}$ from which $IDR_{pmax}$ is computed for the 5, 10, 15 and 20 stories heights frame models under the action of the three load distributions, and also for the additional 25, 30, 32 and 35 stories heights frame models. The maximum inter-story plastic drift ratio ($IDR_{pmax}$) is also ploted in Figure 29 against heights of the 9m bay width archetype frame models for the three load distributions.

It can be seen that the plastic drift ratios from all load distributions increase with height as in the previous 6 and 7.5 m bay width configurations, and as mentioned previously, this is due the strength degradation owing to the P-delta effects. But, all lines do not show clear change or reduction in slope, and then the plastic drift ratios continue increasing with the same rate in tall frame models till the last one of 35 stories height. The plastic drift ratios in Table 9 do not exceed the limit of 1% of item- 2 in Section 4. Also, the maximum inter-story drift ratios at $\delta_t$ ($IDR_{tmax}$) do not exceed the limit of 2% of item- 1 in Section 4.

**Table 9. IDRpmax computed values for the 9m bay width and 5, 10, 15, 20, 25, 30, 32 and 35 stories heights frame models under the action of the three load distributions**

| Height in terms of number of stories | Inter- story drift ratios x $10^{-2}$ | | | | | | | | |
|---|---|---|---|---|---|---|---|---|---|
| | 1st mode load distribution | | | Multi-mode load distribution | | | Uniform load distribution | | |
| | $IDR_{tmax}$ at δt | $IDR_{ymax}$ at $D_y$ | $IDR_{pmax}$ | $IDR_{tmax}$ at δt | $IDR_{ymax}$ at $D_y$ | $IDR_{pmax}$ | $IDR_{tmax}$ at δt | $IDR_{ymax}$ at $D_y$ | $IDR_{pmax}$ |
| 35 | 1.169 | 0.4005 | 0.7685 | 1.12 | 0.4016 | 0.7184 | 1.044 | 0.4051 | 0.6389 |
| 32 | 1.104 | 0.3925 | 0.7115 | 1.070 | 0.3979 | 0.6721 | 0.9905 | 0.394 | 0.5965 |
| 30 | 1.077 | 0.395 | 0.682 | 1.034 | 0.3912 | 0.6428 | 0.9686 | 0.3996 | 0.569 |

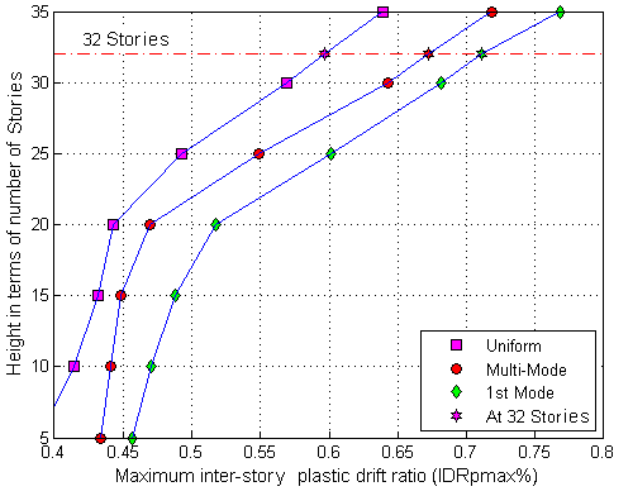


**Figure 29. IDRpmax computed values for the 9m bay width and 5, 10, 15, 20, 25, 30, 32 and 35 stories heights frame models under the action of the three load distributions.**

Table 10 represents the values of the $V_t$, $V_{max}$ and $V_{min}$ for the additional frame models of 25, 30, 32 and 35 stories heights resulted from the action of the three load distributions. The target shear capacity ($V_t$) and the minimum shear capacity ($V_{min}$) were plotted in Figure 30, against the heights of the 9 m bay width archetype frame models for the three load distributions. It is clear that the smallest target shear capacity and the larger target displacement demand are under the effect of the 1st- mode load distribution pattern, which is the worst case among the three load distributions, as in the previous configurations. Also, as the building height increased, the shear capacity decreases and the target displacement increases under the effect of the same earthquake ground motion, this due to the increased P-delta effects in taller (i.e.; heavier ) buildings. But the rate of decrease in target shear is more than that in the minimum shear, and it continues more with height until the target shear capacity becomes equal to and, then less than, the minimum shear capacity.

The target shear capacity ($V_t$) from the 1st- mode load distribution is the only one among those in the other load distributions, reaches and, then be less than, the corresponding minimum shear capacity ($V_{min}$) at an archetype model height just lower than 35 stories. That is why the lines of plastic drift ratios in Figure 29 do not show clear change or reduction in slope, and then the plastic drift ratios continue increasing with the same rate in tall frame models till the last one of 35 stories height.

Anyway, and for the previous reasons which meet item- 3 in Section 4, the 32 stories height will be considered as the maximum limit for the building frames of 9 m bay width.

Also, it can be concluded from the previous sections that the 1st- mode load distribution pattern result in the lowest target shear capacity and the largest target displacement demand, therefore, it mostly was the control load pattern, and as stated in FEMA 440, "the 1st–mode load distribution is recommended ".

**Table 10. The target, maximum and minimum shear values (Vt, Vmax and Vmin) for the 9m bay width and 25, 30, 32 and 35 stories heights frame models under the action of the three load distributions**

| Height in terms of number of stories | Shear values in (kN) | | | | | | | | |
|---|---|---|---|---|---|---|---|---|---|
| | 1st mode load distribution | | | Multi-mode load distribution | | | Uniform load distribution | | |
| | Vt | Vmax | Vmin | Vt | Vmax | Vmin | Vt | Vmax | Vmin |
| 35 | 589.5 | 749.4 | 599.5 | 652.9 | 799.6 | 639.7 | 834.1 | 955.6 | 764.5 |
| 32 | 685.6 | 791.7 | 633.4 | 746.8 | 844.7 | 675.8 | 940.4 | 1013.5 | 810.8 |
| 30 | 739.1 | 823.6 | 658.9 | 801.1 | 875.6 | 700.5 | 999.4 | 1051.2 | 841 |
| 25 | 891 | 914 | 731.2 | 956.4 | 972.1 | 777.7 | 1173 | 1178.4 | 942.7 |

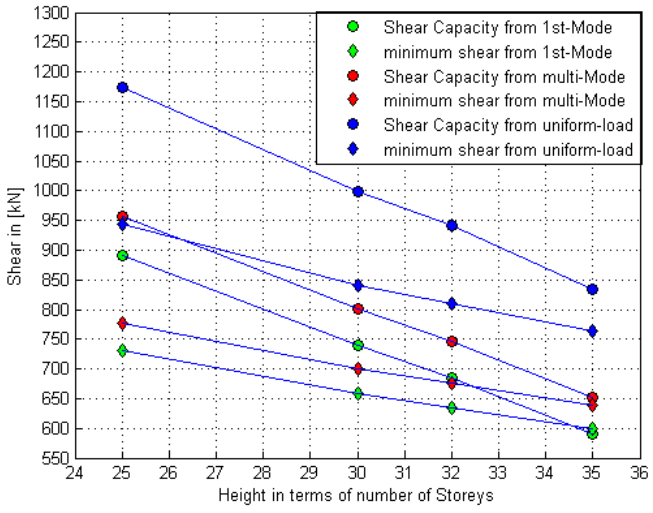


**Figure 30. The shear capacity and minimum shear against the height of 25, 30, 32 and 35 stories heights of the 9m bay width frame models under the action of the three load distributions.**

## 7. General Discussion

In Figure 31, the maximum inter-story plastic drift ratios ($IDR_{pmax}$) for all archetype models of the three groups of the 6m, 7.5 and 9 m bay widths, have been plotted against their heights in terms of number of stories. A comparison between these three groups reveals that in general the plastic drifts increase with decreasing the bay width for any load pattern. Accurately, for a given building height and number of bays, the plastic drifts increase with decreasing the bay

width because the stiffness is decreased and they will be more slender, and consequently, the P- delta effects increased. And, that is why the only 6m bay width archetype model was exceeded the plastic drift limit of 1%, specifically, the 18 stories height model and taller under the action of the 1st- mode and multi- mode load patterns, as clear in Figure 31.

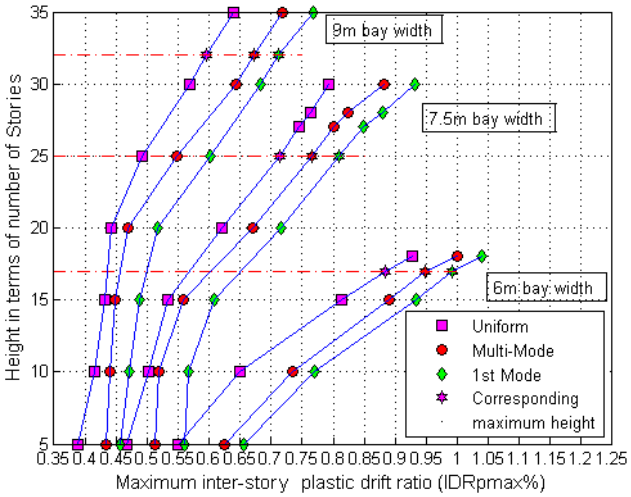


**Figure 31. IDRpmax computed values for all archetype frame models of the 6, 7.5 and 9 m bay widths under the action of the three load distributions**

From discussions of previous sections, it can be summarized that the maximum building heights are 17, 25 and 32 stories for the 6m, 7.5 and 9 m bay widths, respectively. Thus, the maximum building height in terms of maximum number of stories (NSmax) can be plotted against the bay width (B), as shown in Figure 32 for a story height of 4m. It can be noticed that as the bay width increased, the allowed maximum height increased, this is due to the same reasons explained in the previous paragraph. Then, the relation between B and NSmax has defined by the two shown equations. Or, they can be transformed into one second order equation, which is;

$$NS_{max} = \left(\frac{-2}{9}\right) B^2 + \left(\frac{25}{3}\right) B - 25 \,, \qquad \text{for a story height = 4 m} \qquad (8)$$

Where, $NS_{max}$ is rounded to the nearest lowest integer.

Or, for any other bay width between 6 and 9 m, NSmax can be determined by linear interpolation between the surrounding 6m and 7.5m or 7.5m and 9m, whichever the nearest, and then, NSmax is rounded to the nearest lowest integer.

It can be noticed that the lines of IDRs in Figure 31 having their first change in their slope at heights when the shear capacity started to degrade or started to be in the second descending part of the pushover curve. And this can also be concluded from Tables (7.3, 5, 7), where both the $IDR_{ymax}$ and $IDR_{tmax}$ increase with height and then $IDR_{ymax}$ start to stabilize while the corresponding $IDR_{tmax}$ values are continue increasing when the target point (Vt) enters the descending part of pushover curve (the greyed values in Tables) which cause the first change in the slope, i.e, start to stabilize at 10, 15 and 20 stories for the 6, 7.5 and 9 m bay widths which are the same heights of the first change in the slope of corresponding lines.

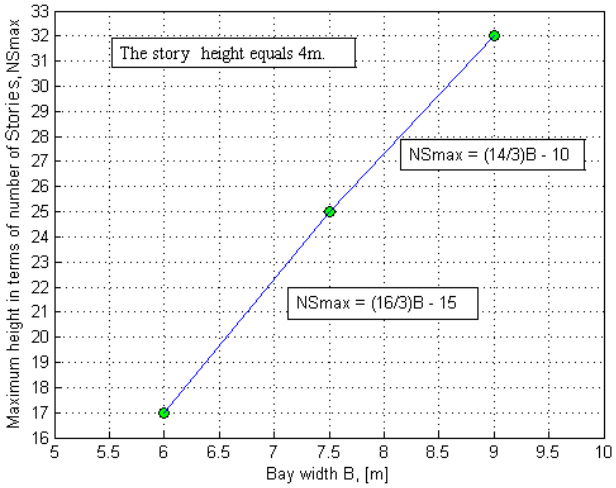


**Figure 32. Maximum building heights in terms of number of stories against the bay width, for a story height of 4m**

## 8. Conclusions

- The 1st mode load distribution pattern result in the lowest target shear capacity and the largest target displacement demand, therefore, it mostly was the control load pattern, and as stated in FEMA 440, "the 1stmode load distribution is recommended ".
- As the building height increased, both, the target and the minimum shear capacities decrease and the target displacement increases under the effect of the same earthquake ground motion, this due to the increased P-delta effects in taller (i.e.; heavier ) buildings.
- For a given building height and number of bays, the plastic drifts increase with decreasing the bay width because the overall building stiffness is decreased and it will be more slender, and consequently, the P- delta effects increased.
- The allowed maximum height of a framed building increased as the bay width increased, because the overall building stiffness will be increased. And it is concluded that the maximum allowed heights of framed buildings are 17 stories, 25 stories and 32 stories for 6, 7.5 and 9 m bay widths, respectively. For any other bay width between 6m and 9m, the maximum allowed height can be determined by linear interpolation between the surrounding 6 and 7.5 or 7.5 and 9 m, whichever the nearest, and then, it is rounded to the nearest lowest integer. All that based on design and reinforcement detailing requirements of the ACI 318- 14, and basing on columns sections sized so that their axial load intensity not to exceed the corresponding intensity at balance point on their moment- load interaction diagram.

## 9. Conflict of Interest

The authors declare no conflict of interest.

## 10. References

[1] AbdulMuttalib Isa Said and Mustafa Shakir Farman, "Re-evaluations of seismic hazard of Iraq", Arabian Journal of Geosciences, 11(11) (June 2018) :1-19. doi: 10.1007/s12517-018-3558-7.

[2] Farman, Mustafa Shakir, and AbdulMuttalib Isa Said. "Updated Probabilistic Seismic Hazard Assessment for Iraq/2018." Civil Engineering Journal 4, no. 7 (July 30, 2018): 1610. doi:10.28991/cej-0309199.

[3] NIST (2016), " Seismic Design of Reinforced Concrete Special Moment Frames: A guide for practicing engineers, NEHRP Seismic Design Technical Brief No. 1, Second Edition, NIST GCR 16-917-40, produced by the Applied Technology Council and the Consortium of Universities for Research in Earthquake Engineering for the National Institute of Standards and Technology, Gaithersburg, MD. https://nvlpubs.nist.gov/nistpubs/gcr/2016/NIST.GCR.16-917-40.pdf.

[4] ASCE 7-5, "Minimum Design Loads for Buildings and Other Structures", American Society of Civil Engineers, Reston, Virginia, (2005).

[5] Iraqi Seismic Code Requirements for Buildings, Code 2016, 1st edition, C.O.S.Q.C., Baghdad, Iraq.

[6] Iranian Code of Practice for Seismic Resistant Design of Buildings (2007), Standard No. 2800, 3rd Edition, Building and Housing Research Center, Tehran, Iran.

[7] TEC, "Specification for Buildings to be Built in Seismic Zones", Turkish Earthquake Design Code, Turkish Republic, Ministry of Public Works and Settlement, Ankara, (2007). http://www.staticad-yigma.com/download/2007_Turkish_Earthquake_Code.pdf

[8] FEMA P-695, "Quantification of building seismic performance factors", prepared by the Applied Technology Council (ATC) for the Federal Emergency Management Agency, Washington, DC, (2009b).

[9] Haselton, C.B., Deierlein, G.G., "Assessing Seismic Collapse Safety of Modern Reinforced Concrete Moment-Frame Buildings", PEER Report 2007/08, Pacific Earthquake Engineering Research Center, College of Engineering, University of California, Berkeley, February 2008. https://peer.berkeley.edu/sites/default/files/web_peer708_curt_b._haselton_gregory_g._deierlein.pdf.

[10] ICS 91.080.040 (2016), "Criteria for Structural Safety of Tall Buildings", Bureau of Indian Standards, Draft Indian Standard. http://www.bis.org.in/sf/ced/CED38(10639)_26082016.pdf.

[11] IS 1893 (Part 1), "Criteria for earthquake resistant design of structures", Bureau of Indian Standards, Indian Standard No. 1893, Part 1: General provisions and buildings. http://rahat.up.nic.in/sdmplan/Earthquake/AnnexureI-V/AnnexureI_Bldg.%20Earthquake.pdf.

[12] ACI Committee 318,"Building Code Requirements for Structural Concrete (ACI 318-14) and Commentary, (ACI 318R-14)", American Concrete Institute, Farmington Hills, Michigan, (2014). http://uoqasim.edu.iq/e_Learning/lec_file/ACI%20318R-14.pdf.

[13] ASCE/SEI 41-13 (2014), "Seismic evaluation and retrofit of existing buildings", American Society of Civil Engineers, Reston, Virginia. https://www.academia.edu/35725359/ASCE_41_13_Seismic_Evaluation_and_Retrofit_of_Existing_Buildings.

[14] Elwood, K. J., Matamoros, A. B., Wallace, J. W., Lehman, D. E., Heintz, J. A., Mitchell, A. D., Moore, M. A., Valley, M. T., Lowes, L. N., Comartin, C. D., and Moehle, J. P. (2007), "Update to ASCE/SEI 41 concrete provisions", Earthquake Spectra, 23 (3): 493 – 523. https://peer.berkeley.edu/sites/default/files/asce_41_update_peer_report_02.pdf.

[15] ETABS, "Technical Note: Material Stress-Strain Curves", Computers and Structures, Inc., june 2008.

[16] ETABS, "Structural and Earthquake Engineering Software", Release 2016, Computers and Structures, Inc.

[17] ETABS, "CSi Analysis Reference Manual", Computers and Structures, Inc., Berkeley, California, USA, copyright 2016.

[18] FEMA 356 (2000), "Prestandard and Commentary for Seismic Rehabilitation of Buildings", Prepared by the American Society of Civil Engineers for the Federal Emergency Management Agency, Washington, D.C. https://www.fema.gov/media-library-data/20130726-1444-20490-5925/fema_356.pdf.

[19] PEER/ATC 72-1, "Modeling and acceptance criteria for seismic design and analysis of tall buildings", Pacific Earthquake Engineering Research Center (PEER)/Applied Technology Council (ATC) (2010). https://peer.berkeley.edu/sites/default/files/peer-atc-72-1_report.pdf.

[20] FEMA P-750 (2009c), "NEHRP Recommended Seismic Provisions for New Buildings and Other Structures", Part 2, Commentary to ASCE/SEI 7-05. https://cdn.ymaws.com/www.nibs.org/resource/resmgr/BSSC/Part-2_P-750_2009_NEHRP_Reco.pdf.

[21] FEMA 450 (2004b), "NEHRP Recommended Provisions for Seismic Regulations for New Buildings and Other Structures", FEMA 450-2/2003 Edition, Part 2: Commentary, Federal Emergency Management Agency, Washington, D.C. https://tycho.escuelaing.edu.co/contenido/encuentros-suelosyestructuras/documentos/5_encuentro/FEMA/FEMA450-fema450part2a.pdf.

[22] FEMA 450 (2004a), "NEHRP Recommended Provisions for Seismic Regulations for New Buildings and Other Structures", FEMA 450-1/2003 Edition, Part 1: Provisions, Federal Emergency Management Agency, Washington, D.C. https://www.nehrp.gov/pdf/fema450provisions.pdf.

[23] FEMA 440 (2005), "Improvement of Nonlinear Static Seismic Analysis Procedures", prepared by the Applied Technology Council (ATC-55 Project) for the Federal Emergency Management Agency, Washington, D.C. https://www.fema.gov/media-library-data/20130726-1445-20490-9603/fema-440.pdf.

[24] ATC-40, "Seismic evaluation and retrofit of concrete buildings", Prepared by the Applied Technology Council, Rep. No. ATC-40, Redwood City, CA, for the California Seismic Safety Commission (Rep. No. SSC 96-01), (1996).